NASA TECHNICAL NOTE

NASA TN D-2538

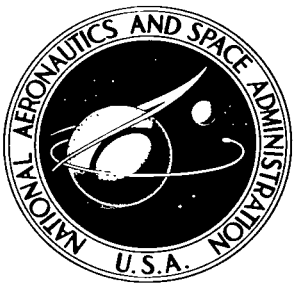

NASA TN D-2538

WIND-TUNNEL INVESTIGATION OF A TILT-WING VTOL AIRPLANE WITH ARTICULATED ROTORS

by James A. Weiberg and Demo J. Giulianetti

Ames Research Center
Moffett Field, Calif.

NATIONAL AERONAUTICS AND SPACE ADMINISTRATION • WASHINGTON, D. C. • MARCH 1965

NASA TN D-2538

WIND-TUNNEL INVESTIGATION OF A TILT-WING VTOL AIRPLANE WITH ARTICULATED ROTORS

By James A. Weiberg and Demo J. Giulianetti

Ames Research Center
Moffett Field, Calif.

NATIONAL AERONAUTICS AND SPACE ADMINISTRATION

For sale by the Office of Technical Services, Department of Commerce,
Washington, D.C. 20230 -- Price $3.00

WIND-TUNNEL INVESTIGATION OF A TILT-WING VTOL AIRPLANE WITH ARTICULATED ROTORS

By James A. Weiberg and Demo J. Giulianetti

Ames Research Center
Moffett Field, Calif.

SUMMARY

The results of the tests showed: (1) a loss of thrust with rotor control input, (2) inadequate lateral-directional control, and (3) severe stall-induced wing and horizontal-tail buffet at the wing angles of attack that would be required in a transition from hover to forward flight.

INTRODUCTION

An investigation was made of the performance and control characteristics of a tilt-wing VTOL airplane with articulated rotors. The airplane (a modified Grumman JRF-5) and the rotor control system were built by the Kaman Aircraft Corporation under contract to the Navy Bureau of Weapons.

The airplane was tested in the Ames 40- by 80-Foot Wind Tunnel to determine the characteristics in the transition speed range from hover to forward flight. The airplane was also tested on a strain-gage support system outside the wind tunnel to determine its hover characteristics near the ground.

NOTATION

a_1 longitudinal flapping, deg

b_1 lateral flapping, deg

b wing span, ft, and number of blades

c rotor blade chord, ft

$\bar{c}$ wing mean aerodynamic chord, ft

C_D drag coefficient including thrust, $\frac{D}{qS}$

C_L lift coefficient, $\frac{L}{qS}$

C_m pitching-moment coefficient, $\frac{M}{qS\bar{c}}$

C_n yawing-moment coefficient, $\frac{N}{qSb}$

C_l rolling-moment coefficient, $\frac{L}{qSb}$

C_Y side-force coefficient, $\frac{Y}{qS}$

C_P power coefficient, $\frac{\text{power}}{\rho n^3 D^5}$

C_T thrust coefficient, $\frac{\text{thrust}}{\rho n^2 D^4}$

D rotor diameter, ft, and drag, lb

J advance ratio, $1.69 \frac{V}{nD}$

L lift, lb, and rolling moment, ft-lb

M pitching moment, ft-lb

n rotor rps

N yawing moment, ft-lb

q free-stream dynamic pressure, psf

S wing area, sq ft

T total thrust, lb

T_o total thrust with zero control input, and total thrust at zero velocity, lb

V velocity, knots

Y side force, lb

α angle of attack of hull reference line, deg

δ cyclic rotor blade flap deflection, deg

δ_o collective blade flap deflection, deg

δ_e elevator angle, deg

δ_f wing flap deflection, deg

δ_s spoiler deflection, deg

η propeller efficiency, $J \frac{C_T}{C_P}$

η' rotor efficiency, $\frac{\eta}{2} + \sqrt{\left(\frac{\eta}{2}\right)^2 + \left(0.8 \frac{C_T^{3/2}}{C_P}\right)^2}$

θ attitude of hull reference line with respect to horizontal and rotor blade angle at 0.75 R, deg

ρ mass density of air, slugs/cu ft

σ solidity ratio, $\frac{2bc}{\pi D}$

τ tilt of wing with respect to hull reference line, deg

ψ angle of yaw, deg

DESCRIPTION OF THE AIRPLANE

General

The airplane geometry and dimensions are given in figure 1 and table I. The airplane is shown in the tunnel in figure 2 and on the ground test stand in figure 3. The wing could be tilted 62.2° at a rate of approximately 5° per second. The wing had full-span (except for the fuselage and nacelles) 40-percent-chord Fowler-type flaps that could be deflected 40°. The geometry of the cambered nose flap and leading-edge slat used for some of the tests is shown in figure 1(b). The aerodynamic controls on the airplane (fig. 1(a)) consist of elevators, a rudder, and spoilers.

Rotors

The airplane was equipped with two 3-bladed articulated rotors driven through a reduction gear box by two 1025 hp free-turbine engines interconnected by a cross shaft in the leading edge of the wing. The rotor blades could flap about a hinge offset 9.2 percent of the blade radius from the shaft axis. Spring restraints were provided in the lead-lag direction. The blades had a negative pitch-flap coupling of -0.6 ($\delta_3 = -30°$). Blade flapping in the direction to increase coning resulted in a blade pitch change that increased thrust; each 1° of flapping gave a 0.6° blade pitch change. The blades could be rotated about the 25-percent chord line to provide collective blade pitch. The rotor was not provided with cyclic blade pitch control. Cyclic control of the blades was obtained by deflecting large flaps (0.5 chord, 0.4 span). These flaps differed from the servo-tab or external-type flaps

used on some helicopters in that they were built into the blade itself to form a plain-type flap. Collective or cyclic deflection of these flaps was through linkages connected to a swash plate. The rotor flap control system is shown in figure 4. The control advance angle was 58° (i.e., peak blade flap deflection was at a rotor azimuth angle of 58°).

Flight Controls

The flight controls for the airplane were designed as a combination of aerodynamic and rotor controls. However, for the tests reported herein, the elevator and rudder characteristics were investigated separately from the rotor. During tests of the rotor control effectiveness, the elevator and rudder were disconnected from the control system and locked at 0° deflection. Thus, for the rotor control tests, longitudinal and directional control input produced cyclic deflection of the blade flaps and lateral control produced spoiler deflection and differential collective blade pitch. Because wing tilt introduces a lateral-directional control moment conversion (e.g., rolling moment from differential collective blade pitch with wing up converts to yawing moment, wing down), the airplane control system incorporated linkages to provide compensating controls with wing tilt, as shown in figure 5, to give more nearly pure airplane rolling and yawing moments with control input.

TESTS AND CORRECTIONS

Test Variables

In most of the wind-tunnel tests the angle of attack was varied while wing tilt, power, propeller rpm, and tunnel velocity were held constant. The tests were made for a range of wing tilt angles from 0° to 50° and tunnel velocities from 20 knots (1.5q) to 150 knots (75q).

Thrust Calibration

Propeller thrust was determined with the airplane at 0° angle of attack with the wing down and the flaps up. Thrust was assumed to be the sum of the measured longitudinal force with propellers on and the measured drag with propellers off. The engines were not equipped with torque meters; instead power was determined from manufacturer's engine calibration curves and measured engine rpm, air pressure, and temperature.

Corrections

The data presented include the direct propeller forces as well as the aerodynamic forces. The forces were computed relative to the wind axis and the moments relative to the stability axis for the center-of-gravity location shown in figure 6. No corrections have been made for the influence of the tunnel walls or support struts.

Static Stand Tests

Hover characteristics near the ground (fig. 3) were determined from tests with the airplane on a static stand outside the wind tunnel. The fuselage was set at an attitude of 14.1°. The wing trailing edge was approximately 5.5 feet above the ground with the wing tilted and the flaps down 40°.

The airplane was mounted on a strain gage support system that measured vertical and longitudinal forces. Side force could not be measured but was assumed to be the side force component of the propeller thrust (i.e., $T \sin b_1$, where T = total thrust and b_1 = lateral tilt of the rotor determined from oscillograph records of blade flapping). In addition it was assumed that the total side force was supported by the two front struts (fig. 3) and that the tail support strut, which was free to gimbal, did not restrain the model in yaw. Measurements made when the model was in the wind tunnel on the six-component balance proved this assumption to be reasonable (fig. 7).

The tests on the static stand were made with the wing at 0° and 62.2° tilt and for a range of flap deflections from 0° to 40°.

RESULTS AND DISCUSSION

Rotor Characteristics

Thrust.- Thrust was determined for a range of airspeeds from 0 (static stand tests) to 150 knots, a range of blade angles from 6° to 33°, and a range of collective blade flap deflections from 2° to 12°. The results are presented in figure 8. The system efficiency which includes transmission losses is presented in terms of normal propeller efficiency $\eta[J(C_T/C_P)]$ as well as rotor efficiency η' which includes a static figure of merit term $[0.8(C_T^{3/2}/C_P)]$. This expression for η', defined in the notation, is equivalent to a figure of merit at 0 forward speed, and approaches the normal propeller efficiency η with increasing speed (fig. 8(c)). Estimated transmission losses of 8.7 percent were used to determine rotor efficiency from the system efficiency. Rotor efficiency was low (approximately 0.65) and nearly constant with velocity. Thrust decreased rapidly with forward speed

(fig. 8(c)). The blade flap did not appear to be very effective in providing efficient rotor performance over the speed range. Blade pitch was as efficient as blade flap deflection in obtaining a given thrust (fig. 8(a)). The effect of blade flap deflection was to reduce the blade pitch for a given thrust.

Tests were made to determine rotor instability by tilting the wing. No instability (similar to that reported in ref. 1) was noted at speeds up to 150 knots. The blade flapping variation with angle of attack (fig. 9) was close to that estimated from reference 2.

Rotor control effectiveness.- The ability of the rotor to provide adequate control was determined for the airplane in the hover configuration on the static stand and in the transition speed range in the wind tunnel. The results are presented in figures 10 to 18.

In the tunnel tests the control characteristics were determined separately for the aerodynamic and rotor controls because of buffet induced rotor oscillations. The horizontal tail was stalled at 0° fuselage angle of attack and above at all speeds in the transition, resulting in buffet loads on the tail of $\pm 1g$. The resulting buffet of the elevator and rudder were fed back into the rotor control system through the cockpit controls resulting in an irregular weaving motion of the rotor. Because of this feedback, the elevator and rudder were disconnected and locked out of the control system during cyclic rotor control excursions.

A measure of the adequacy of the rotor control power was obtained by comparison with the recommendations of reference 3 for control power in hover for V/STOL aircraft. These control requirements have been converted to control moment for a given control input by means of the estimated airplane inertia characteristics in table I. These recommended control moments are shown in figures 10, 15, and 16 for comparison with the measured results in hover on the static stand ($\tau = 62.2^{\circ}$). Based on the recommendations of reference 3, the rotor provides adequate longitudinal control for hover but lacks sufficient lateral and directional control. Additional directional control might be obtained by increasing the amount of lateral cyclic blade flap deflection for a given control input. However, the nonlinearity of the moment curves indicates a decrease in blade flap effectiveness even at moderate flap angles.

The structural deformation of the blades or of the blade flaps which were quite flexible may contribute to the ineffectiveness of the blade flaps and may affect rotor performance. No measurements were made of this deformation on the operating rotor and a stiffer flap was not tested to determine whether the effectiveness could have been improved.

The data in figures 15 to 18 show that the lateral-directional control moment conversion with wing tilt was not completely compensated to give pure rolling and yawing moments. Part of this lack of control compensation may be due to the low effectiveness of the controls.

Figures 10 to 18 show that rotor cyclic control input at constant power produced variations in lift and drag indicative of a thrust loss with control input. The results of calculations of rotor performance with a flap type cyclic control, based on the methods of reference 4 indicated a similar thrust variation with control input (fig. 19).

Airplane Characteristics

Hover.- The variation of lift, drag, and pitching moment with engine power with the wing at its maximum tilt position (62.2°) and with various flap deflections is shown in figure 20. This figure shows that the thrust obtainable with the installed power of 2050 hp is sufficient for hovering with a gross weight of 9000 lb. Turning angles computed from the data in figure 20 are presented in figure 21. Values estimated by the method of reference 5 are included in figure 21 and are about 12 percent higher than those measured at rated rotor speed of 725 rpm. The turning effectiveness determined from tests of a 1/8-scale model (ref. 6) was between these values.

Transition.- The wing attitude, power, and rotor control required for unaccelerated level flight in the transition are shown in figure 22. These data were obtained from the data in figures 23 to 27 and are for an airplane gross weight of 9300 lb. The wing angles of attack required were close to those measured in small-scale tests (ref. 6). Below approximately 35 knots, the power required (for a 9300 lb airplane) exceeds the total installed power of 2050 hp.

The cyclic control available was severely limited by mechanical interference in the swash plate linkage. Most of the available control (0.6 of design value) was required for balancing the airplane in level flight and little or none remained for maneuvering.

The airplane became statically unstable (as indicated by dC_m/dC_L) at speeds below 40 knots and wing tilt angles greater than 30°. Reference 7 indicated that lack of adequate static stability can adversely affect pilot opinion of the airplane handling qualities.

Stall.- Tuft studies (fig. 28) showed that one-half or more of the wing was stalled in the transition from 60 knots and 20° wing tilt to 23 knots and 50° tilt. The stall caused severe buffeting of the airplane at the angle of attack for balanced unaccelerated level flight. Most of the tests wherein angle of attack was varied were terminated because of this buffeting. A limited investigation was made with two devices (fig. 1(b)) to alleviate the stall: a drooped leading edge over the outboard 90 percent of the wing span and a slat over the center 10 percent. The results are shown in figures 24 to 27. The drooped leading edge had little beneficial effect since the stall originated on the center section outside the slipstream. The center section slat helped the forward portion of that area but the stall then occurred between the slat and the propeller and spread spanwise.

Rotors off.- The aerodynamic characteristics of the airplane with rotors off are shown in figures 29 and 30 and the elevator control effectiveness, in figure 31. With the fuselage level ($\alpha = 0$) in balanced unaccelerated flight (fig. 25), the horizontal tail is stalled so that the elevator is ineffective for longitudinal control near the forward flight region of the transition where it was intended to supplement the rotor control moment. The effectiveness of the spoilers is presented in figure 32.

CONCLUDING REMARKS

The wind-tunnel tests indicated that the flaps built into the rotor blades were effective for cyclic control; however, cyclic control input caused large thrust losses. The rotor efficiency was low and the rotor thrust decreased rapidly with forward speed. The rotor blade flaps were not effective in improving the rotor efficiency throughout the speed range. For this particular tilt-wing airplane, the lateral-directional control was inadequate and had a lateral-directional control interaction with wing tilt. Severe wing and horizontal-tail buffet occurred at the wing angles of attack required in the transition flight region from horizontal to vertical flight. Rotor oscillations induced from this horizontal-tail buffet in the transition precluded the interconnect of the rotor and the aerodynamic controls.

Ames Research Center
National Aeronautics and Space Administration
Moffett Field, Calif., Sept. 23, 1964

REFERENCES

1. Quigley, Hervey C., and Koenig, David G.: The Effect of Blade Flapping on the Dynamic Stability of a Tilting-Rotor Convertiplane. NASA TN D-778, 1961.

2. Meyer, J. R., Jr., and Falabella, G., Jr.: The Effect of Blade Mass Constant and Flapping Hinge Offset on Maximum Blade Angles of Attack at High Advance Ratios. Proc. 8th Annual Forum American Helicopter Soc., May 1952.

3. Anderson, Seth B.: An Examination of Handling Qualities Criteria for V/STOL Aircraft. NASA TN D-331, 1960.

4. Gessow, A.: Equations and Procedures for Numerically Calculating the Aerodynamic Characteristics of Lifting Rotors. NASA TN 3747, 1956.

5. Kuhn, R. E.: Semiempirical Procedure for Estimating Lift and Drag Characteristics of Propeller-Wing-Flap Configurations for Vertical and Short Take-Off-and-Landing Airplanes. NASA MEMO 1-16-59L, 1959.

6. Burgan, E. T.: Partial Results of Wind-Tunnel Tests of a 1/8-Scale Powered Model K-16B Kaman VTOL/STOL Airplane. TED TMB AD 3251, 1960.

7. Quigley, Hervey C., and Innis, Robert C.; Handling Qualities and Operational Problems of a Large Four-Propeller STOL Transport Airplane. NASA TN D-1647, 1963.

TABLE I.- DIMENSIONS OF THE AIRPLANE

Wing	
Area, sq ft	231
Span, ft	34
Mean aerodynamic chord, ft	6.86
Aspect ratio	5.0
Taper ratio	0.70
Section profile	NACA 23021
Horizontal tail area, sq ft	76
Vertical tail area, sq ft	58
Engine	General Electric YT-58-6
Normal rated	875 hp
Military rated	1025 hp
Rotor	
Diameter, ft	15.17
Disk area, sq ft	181
Solidity,	0.189
Blade chord, ft	1.5
Blade twist	0.339°/in.
Blade section	NACA 16-509
Activity factor per blade	155
Moments of inertia	9300 lb gross weight
Roll I_x	22,000 slug-ft^2
Pitch I_y	13,500 slug-ft^2
Yaw I_z	25,300 slug-ft^2

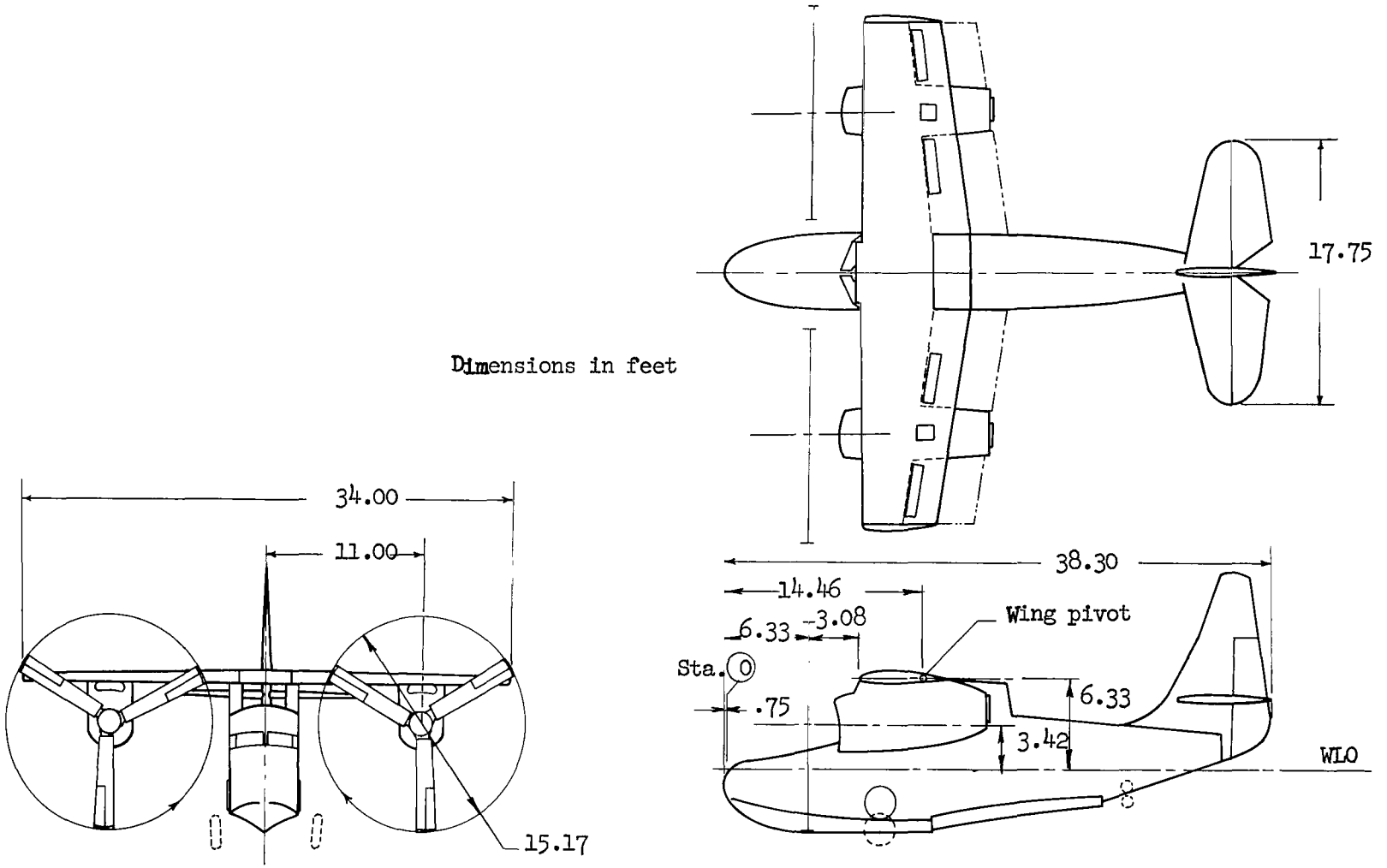

(a) General dimensions.

Figure 1.- The geometry of the airplane.

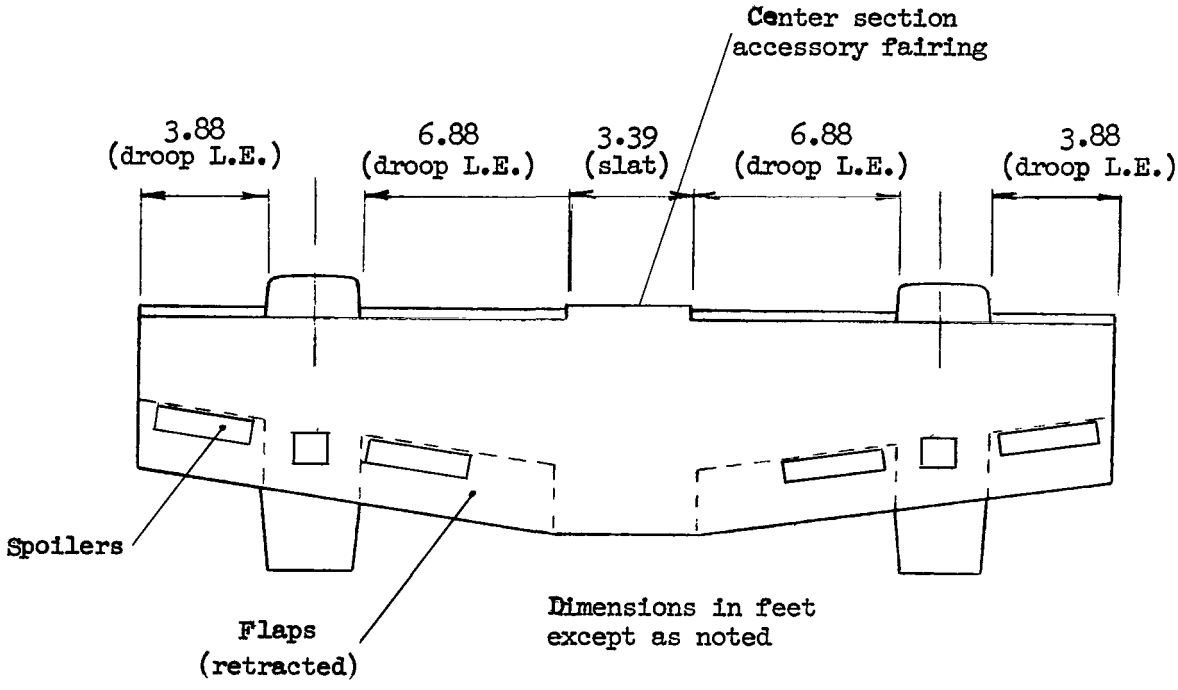

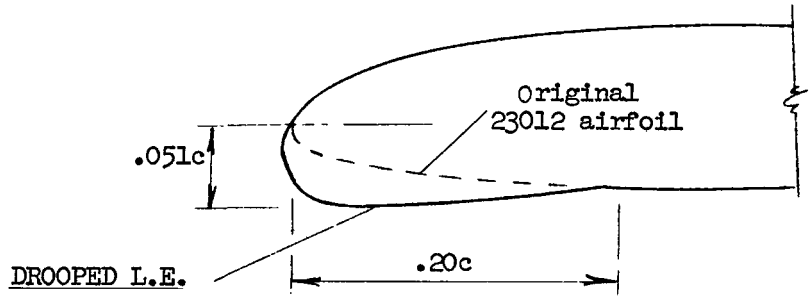

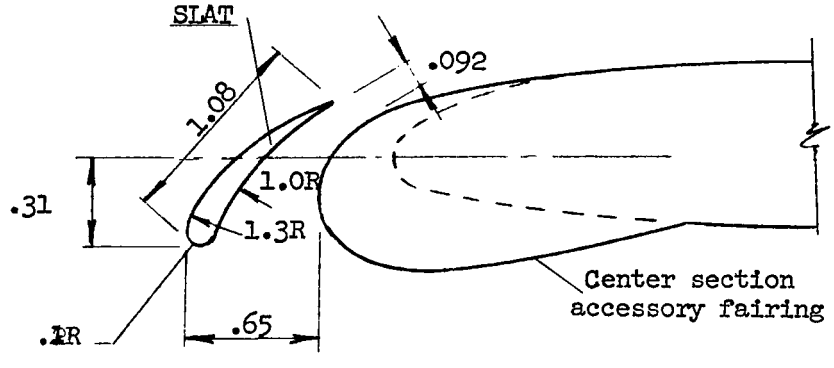

(b) Drooped leading edge and slat.

Figure 1.- Concluded.

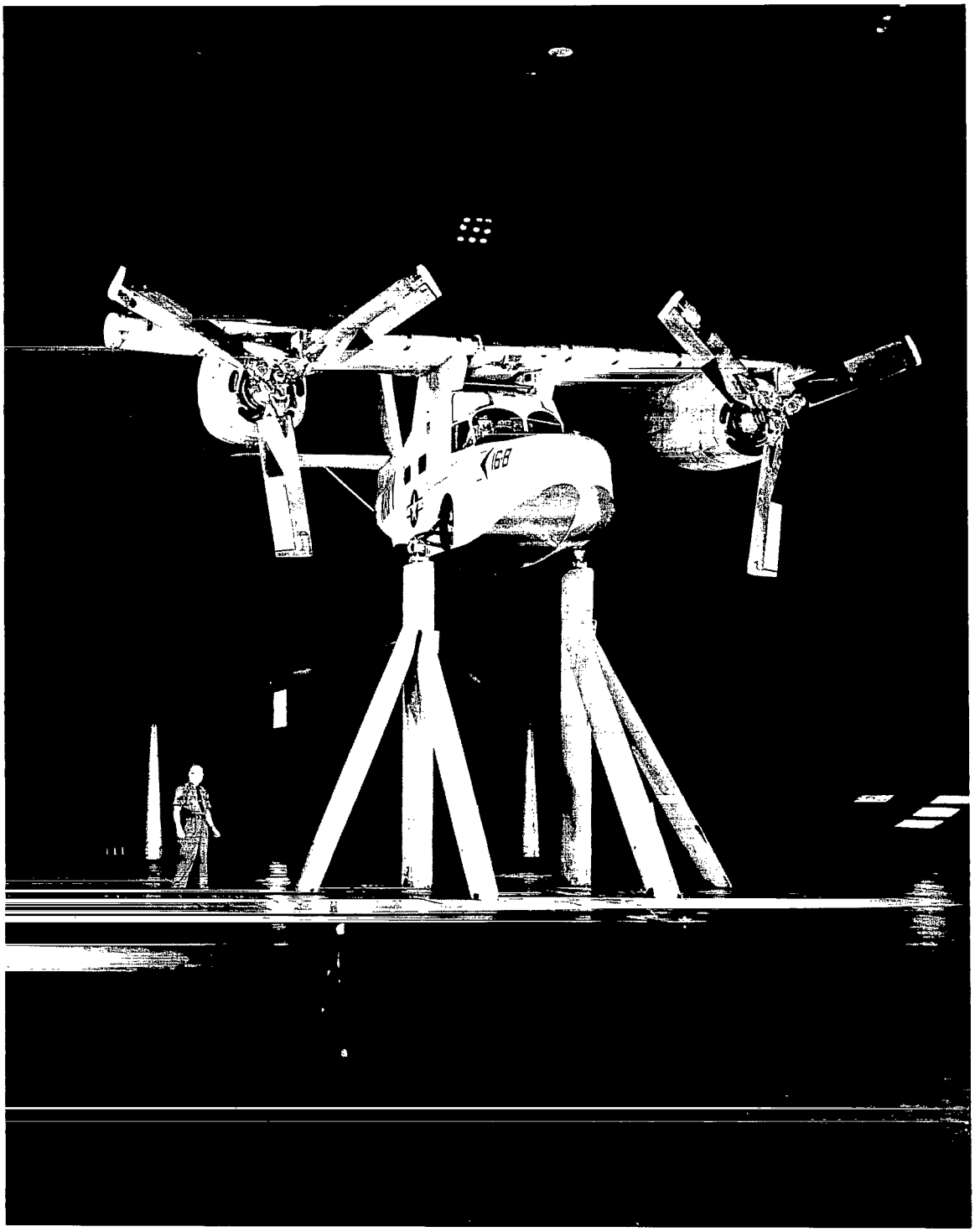

A-29884-1

Figure 2.- The airplane with slat and drooped leading edge mounted in the wind tunnel.

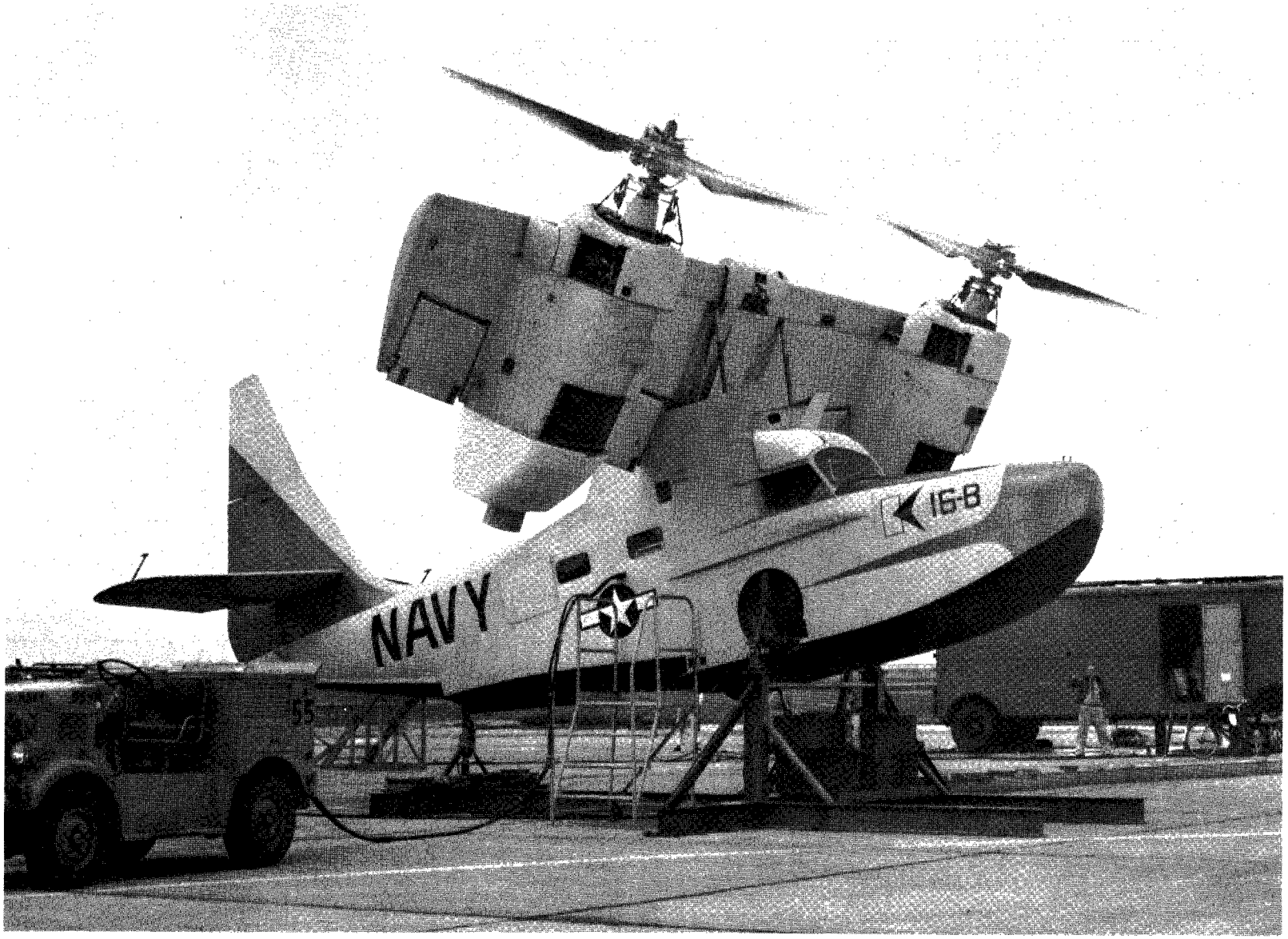

Figure 3.- The airplane on the ground test stand.

A-28910

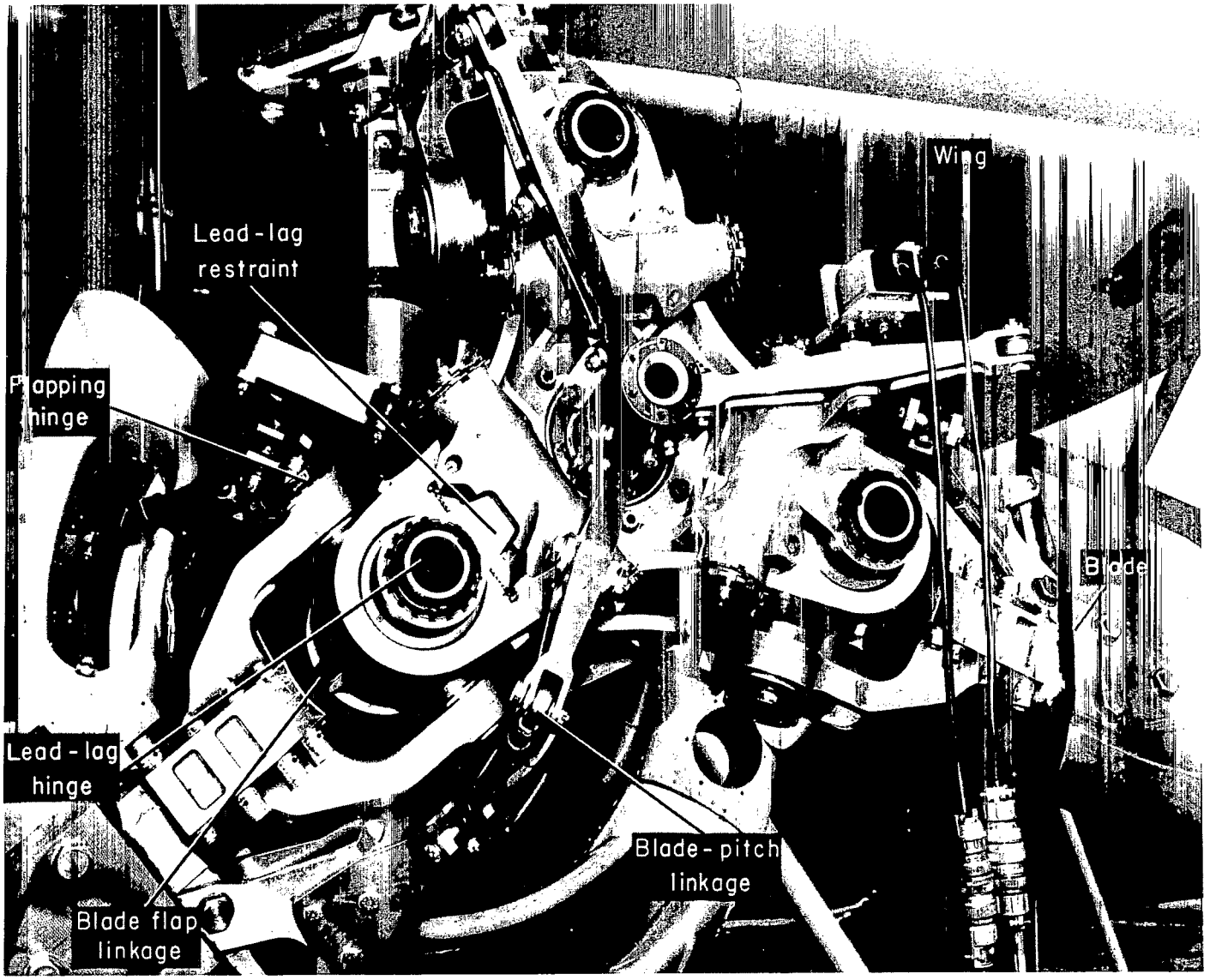

A-28778.1

(a) Front view.

Figure 4.- Rotor hub details.

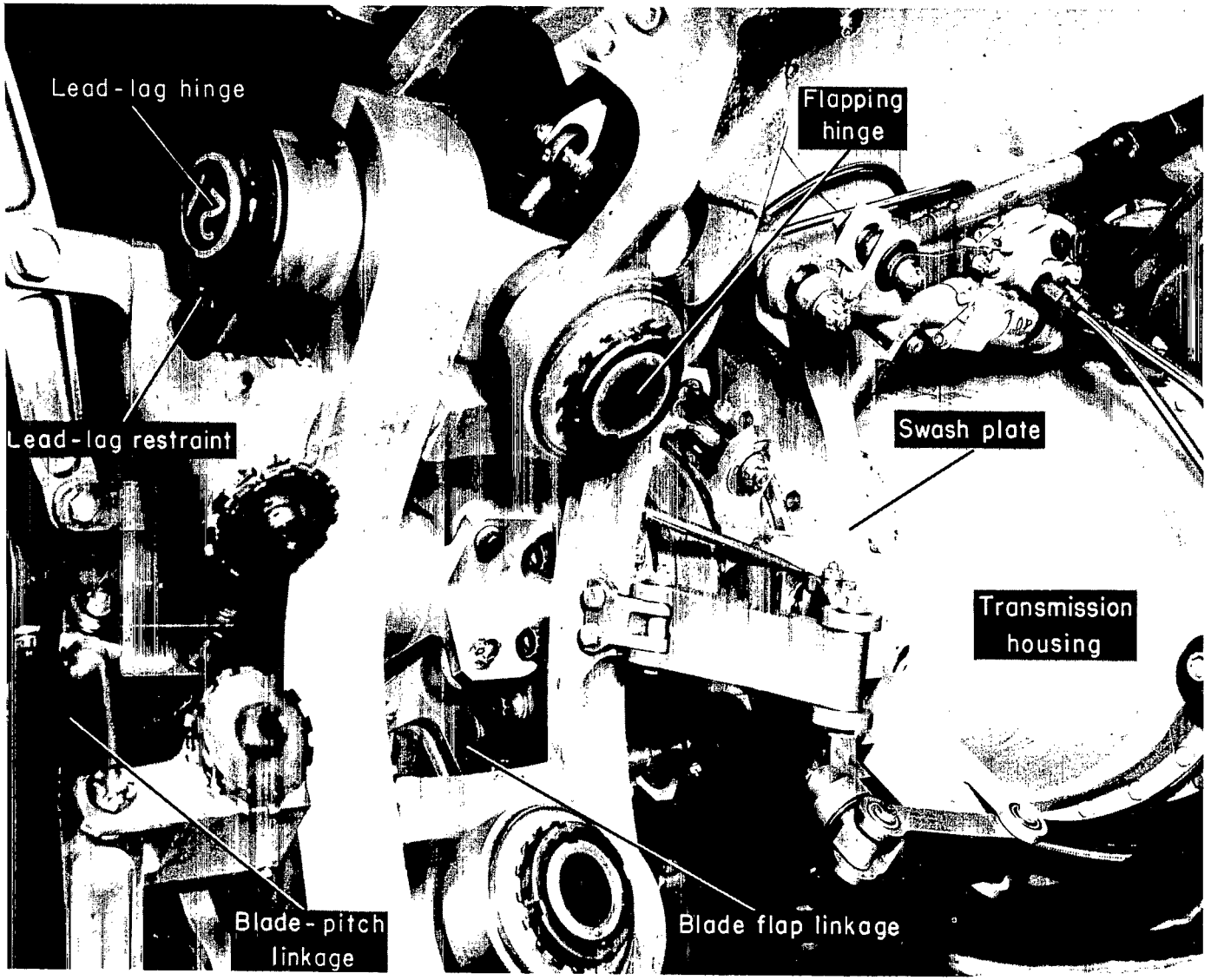

(b) Side view.

A-29385.1

Figure 4.- Continued.

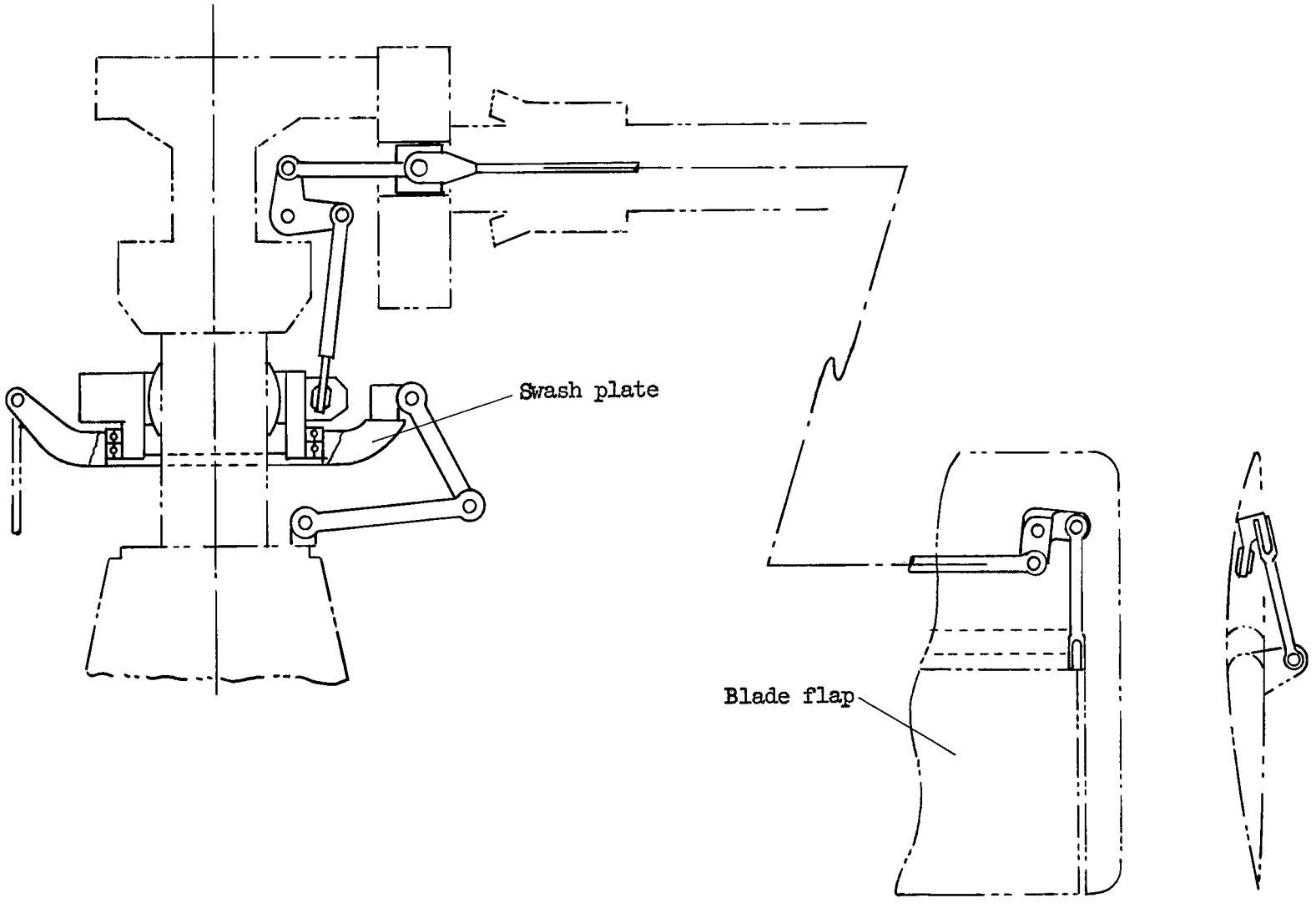

(c) Schematic drawing of blade flap linkage.

Figure 4.- Concluded.

Figure 5.- Rotor control system characteristics.

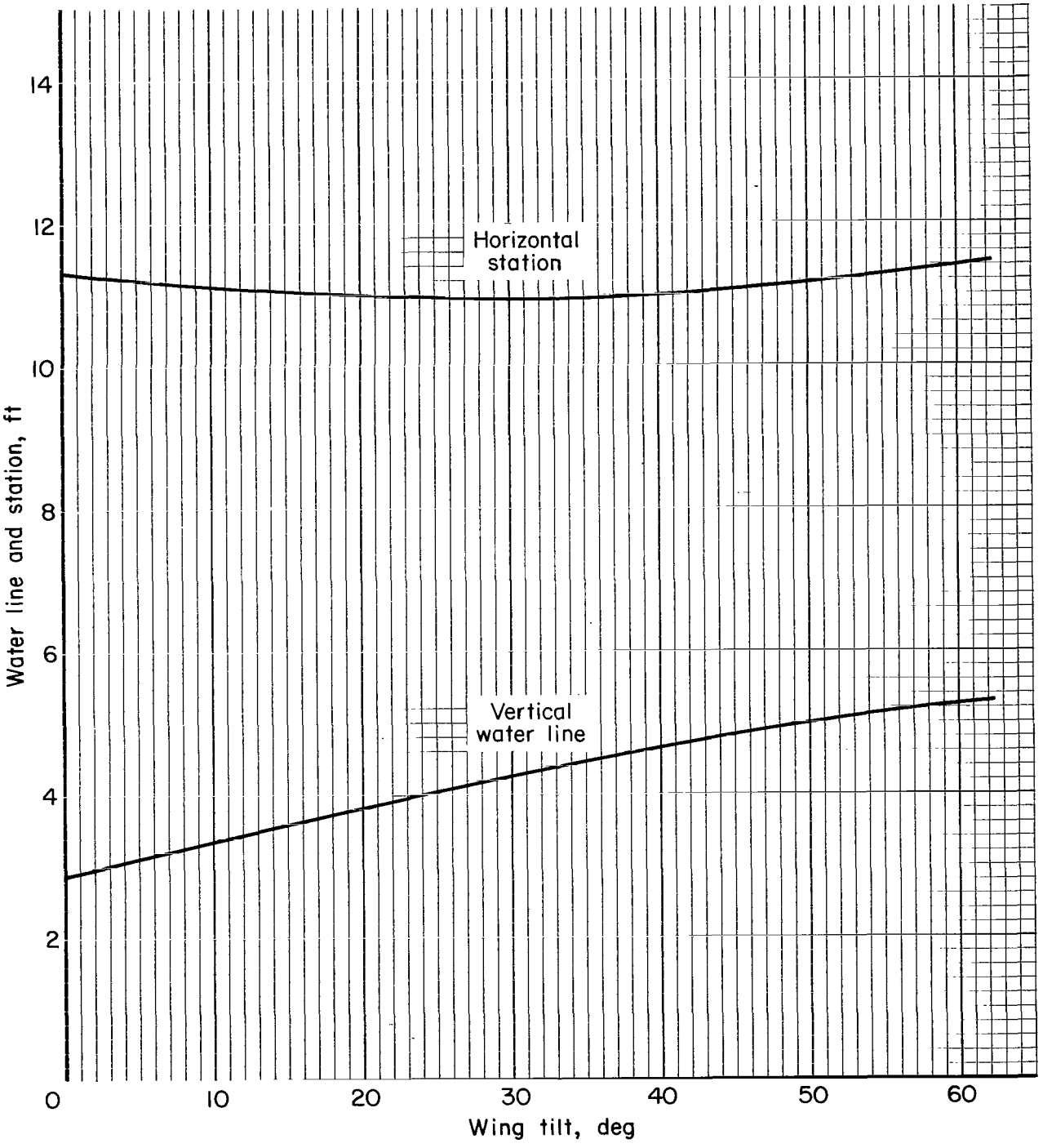

Figure 6.- Center-of-gravity variation with wing tilt.

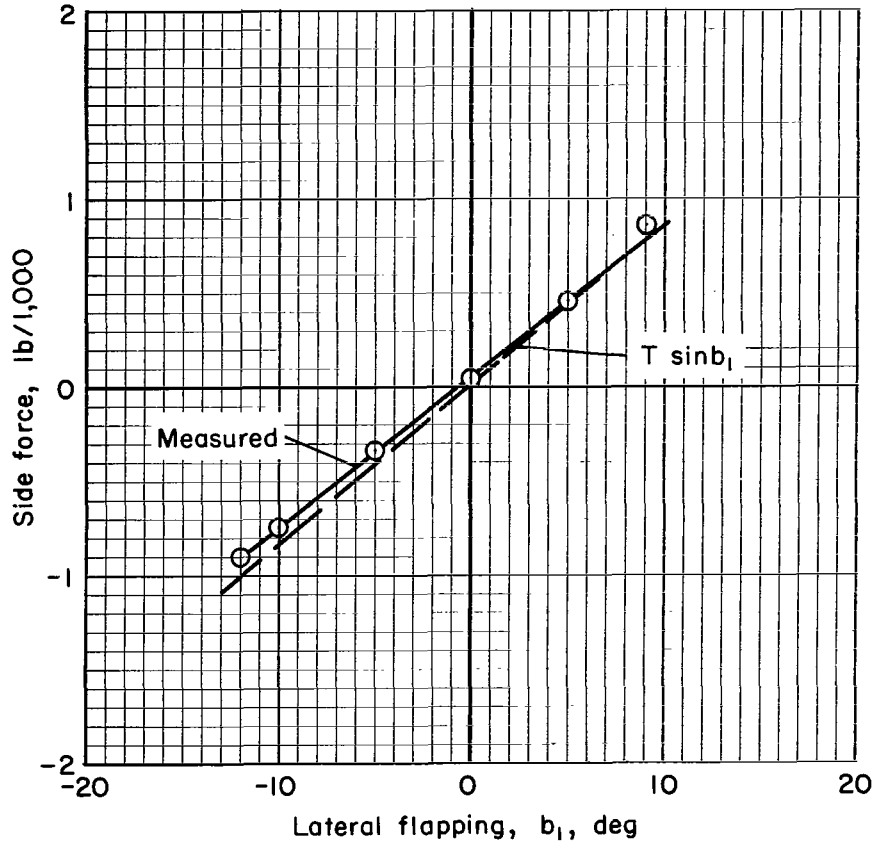

Figure 7.- Comparison between measured side force and side force computed from rotor thrust; $\tau = 40^{\circ}$, $\delta_f = 40^{\circ}$, 1430 hp, 700 rpm, $\alpha = 0$, $\delta_o = 11.7^{\circ}$, V = 40 knots.

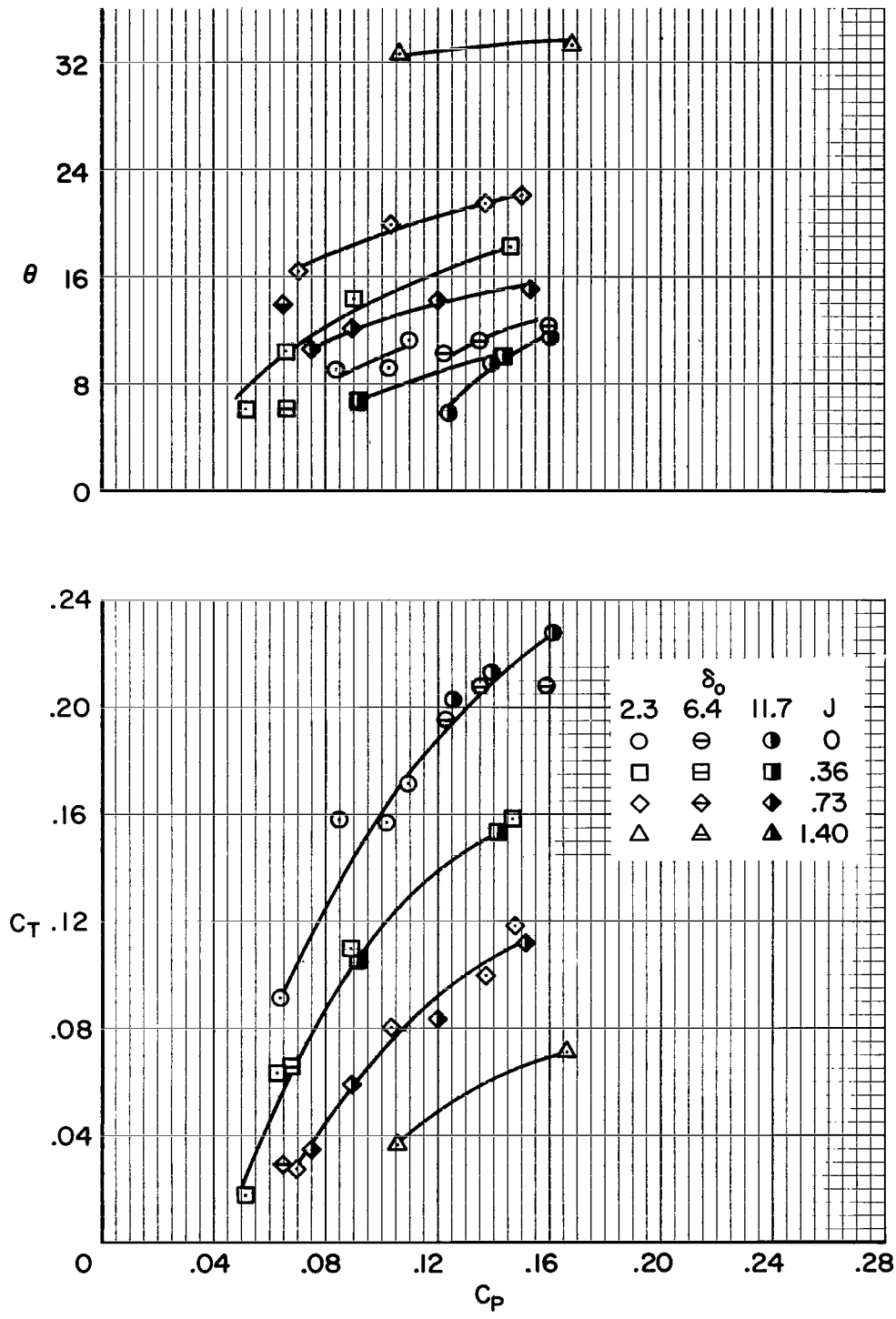

(a) C_T, θ

Figure 8.- Rotor characteristics

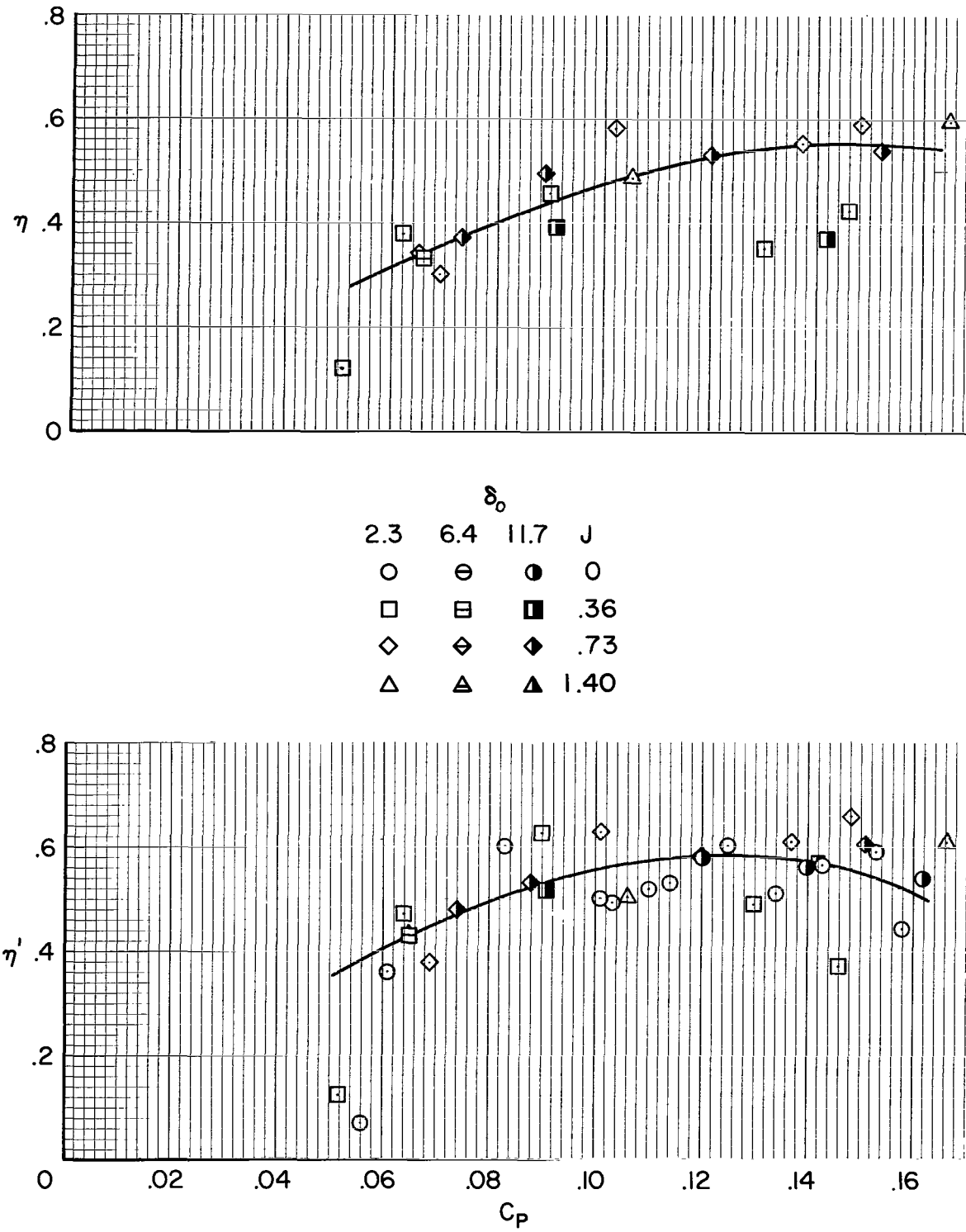

(b) η, η'

Figure 8.- Continued.

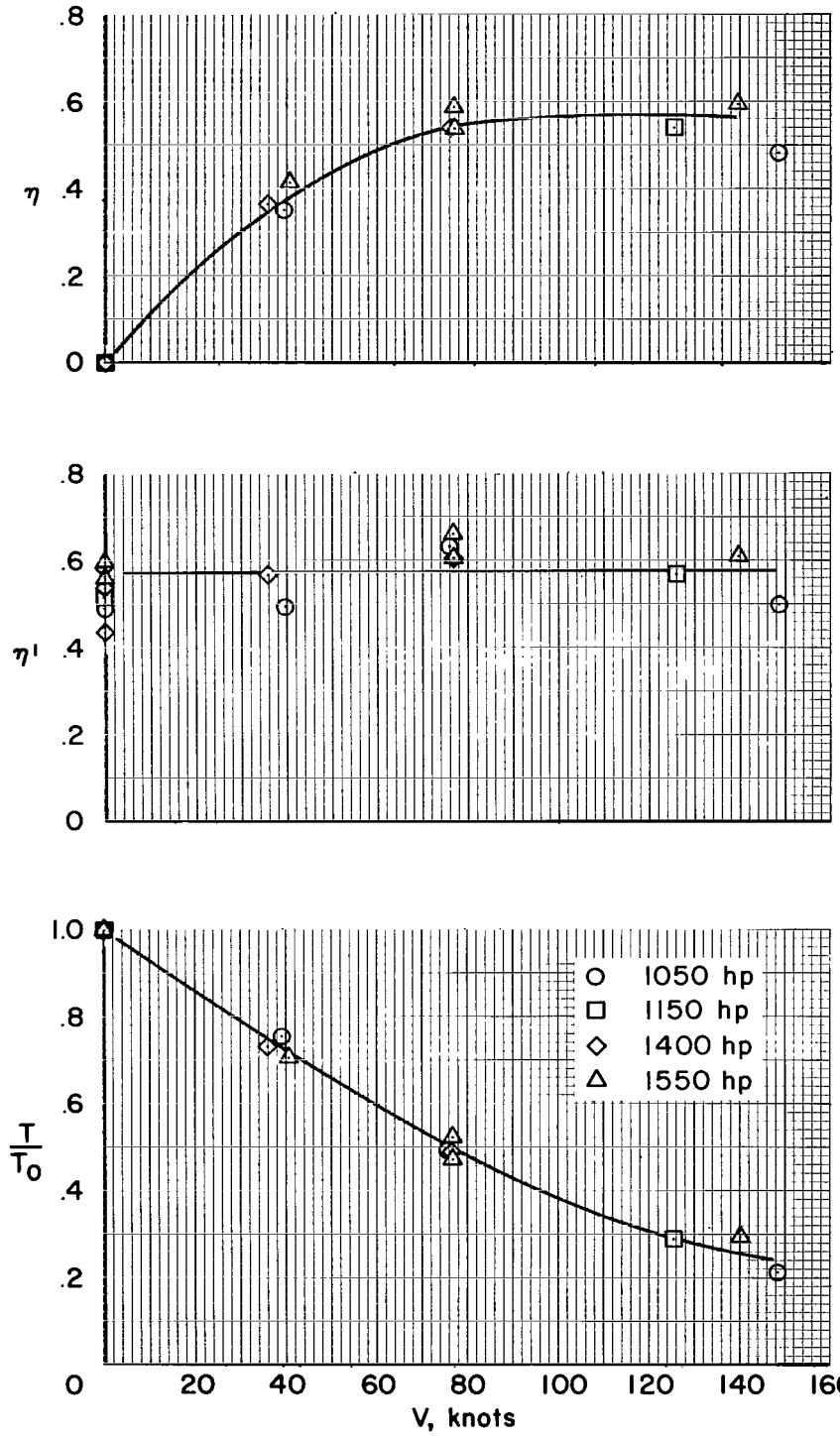

(c) Effect of forward speed.

Figure 8.- Concluded.

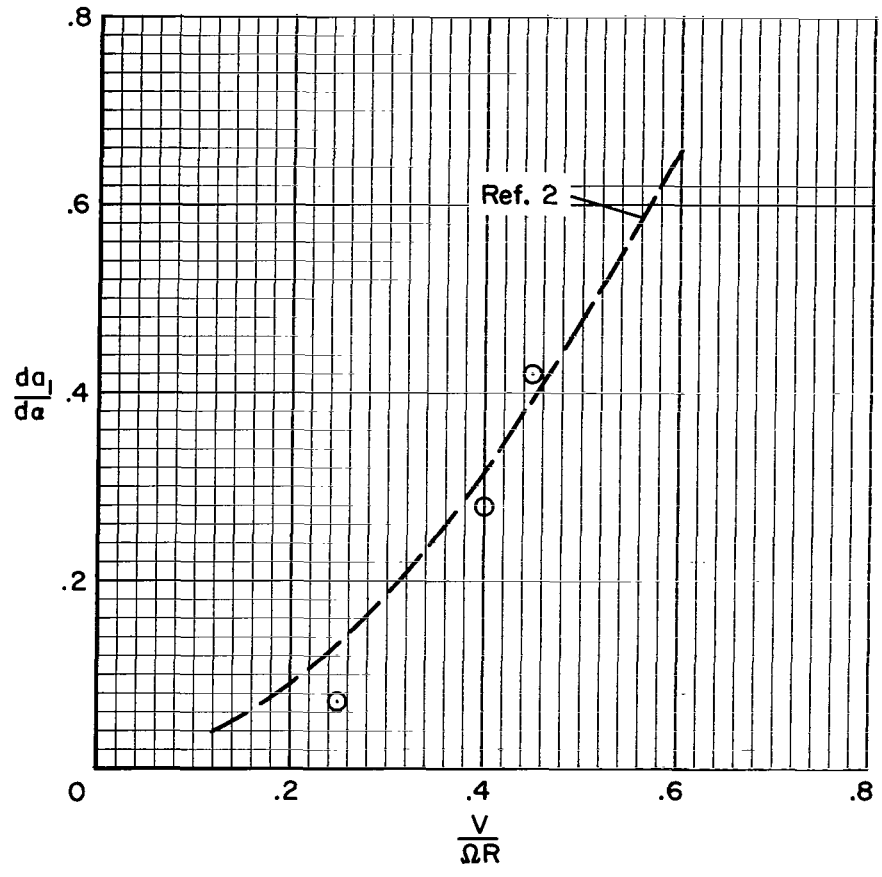

Figure 9.- Rotor blade flapping variation with angle of attack; $\tau = 0$, $\delta_o = 2.3^o$.

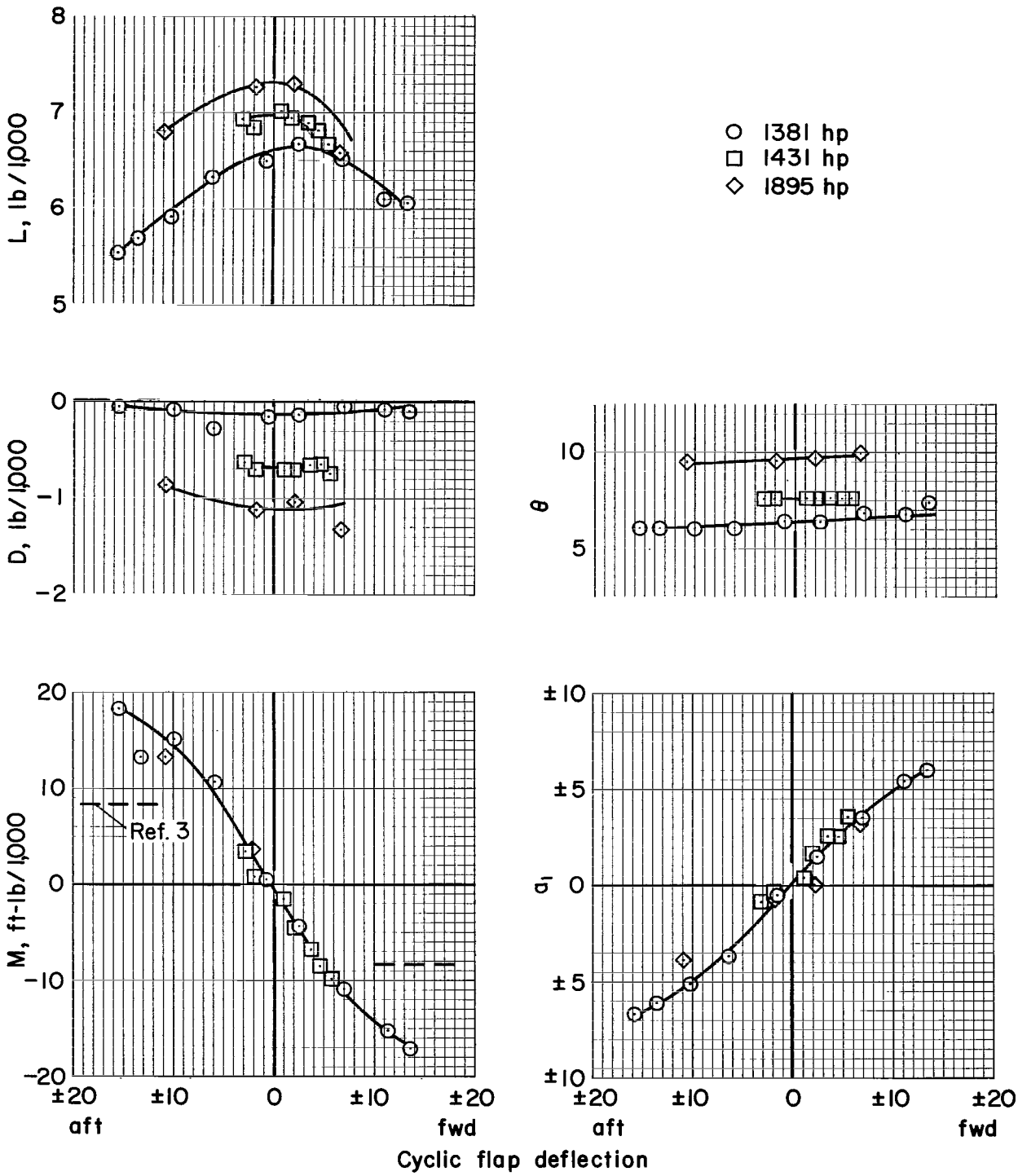

Figure 10.- Longitudinal rotor control effectiveness of the airplane on the static stand; plain L.E., $\tau = 62.2^{\circ}$, $\delta_f = 40^{\circ}$, $\alpha = 14.1^{\circ}$.

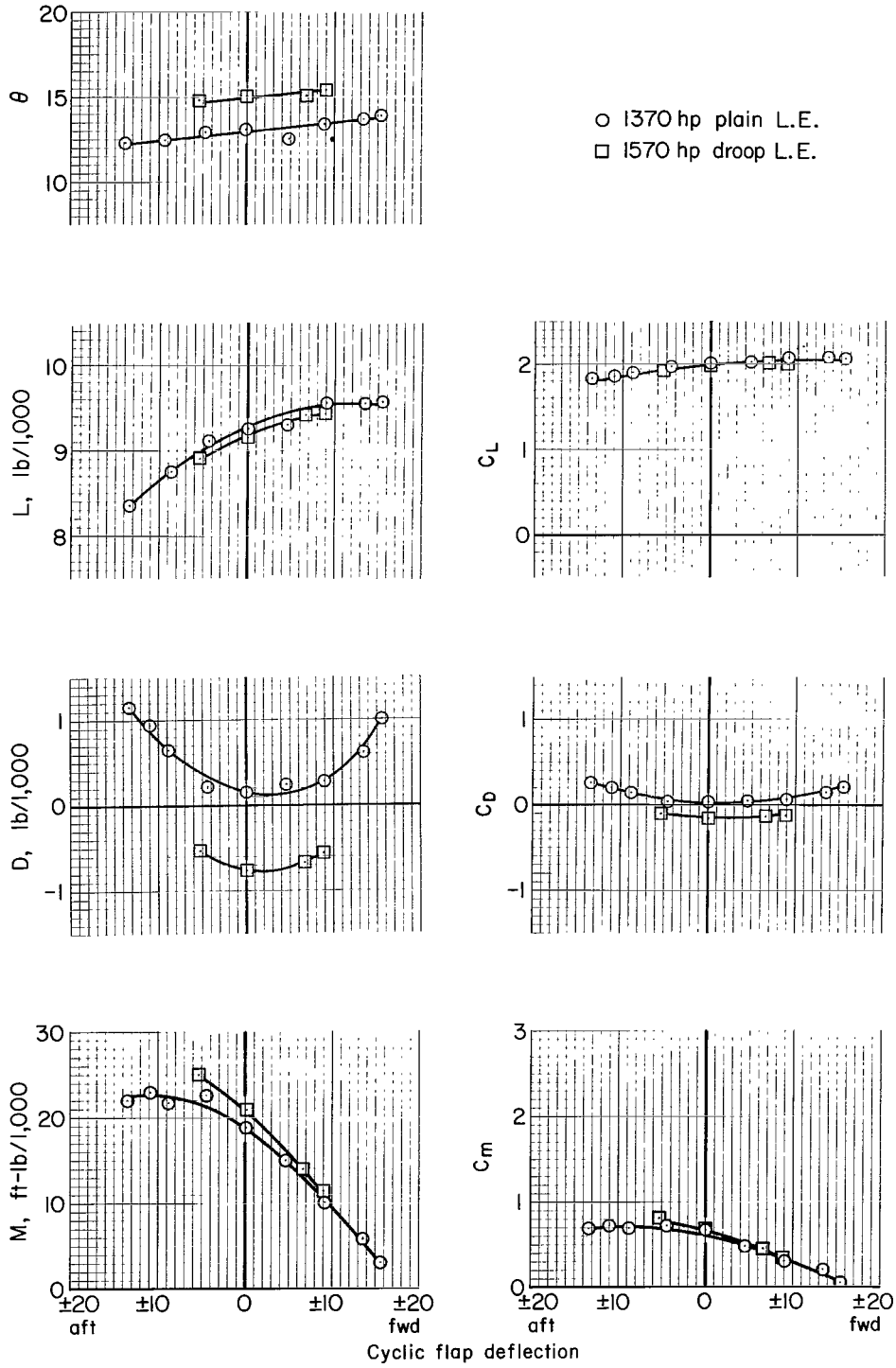

(a) Lift, drag, and pitching moment.

Figure 11.- Longitudinal rotor control effectiveness; $\tau = 10^{\circ}$, $\delta_e = 0$, $\delta_f = 40^{\circ}$, V = 78 knots.

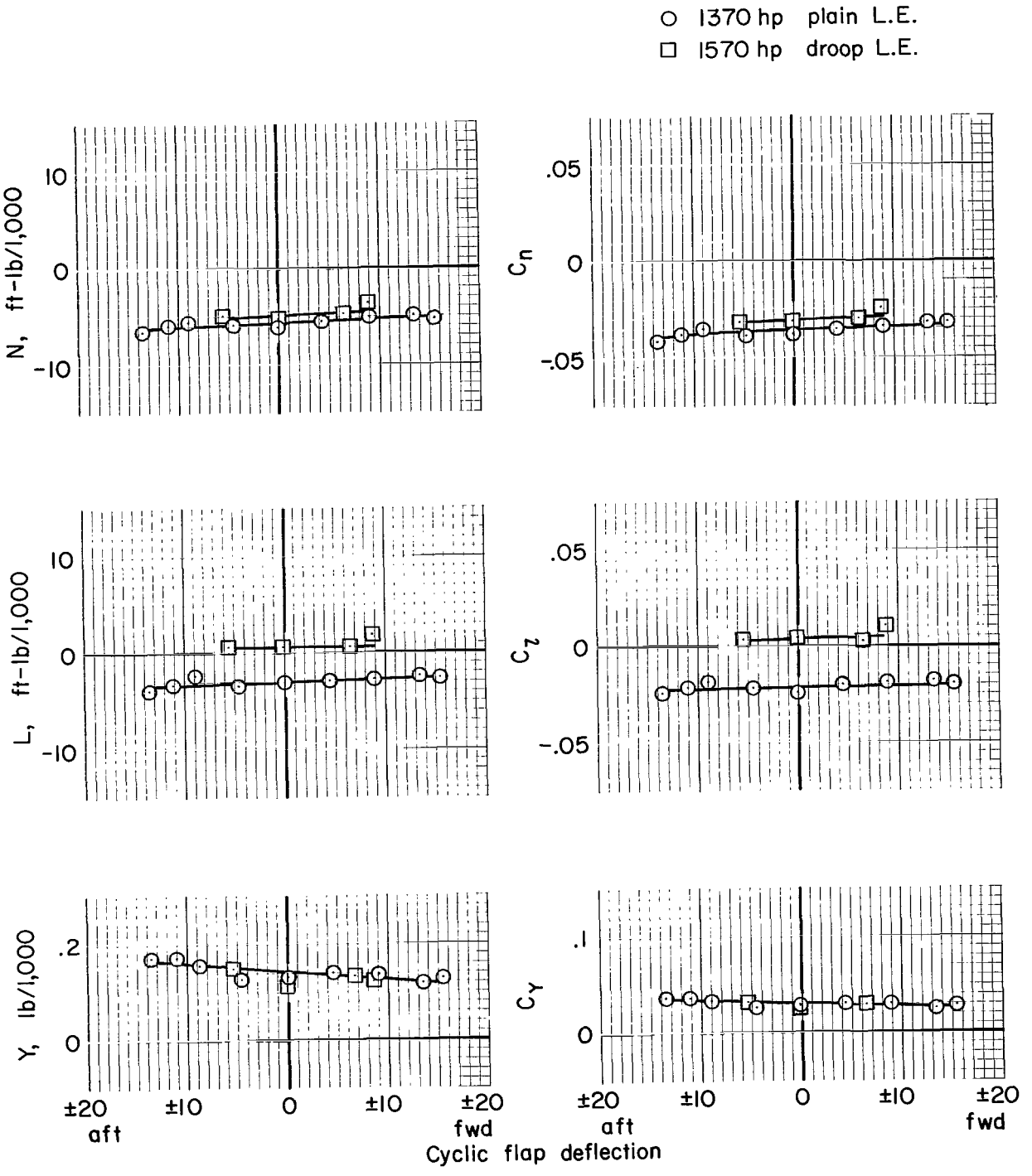

(b) Yaw, roll, and side force.

Figure 11.- Concluded.

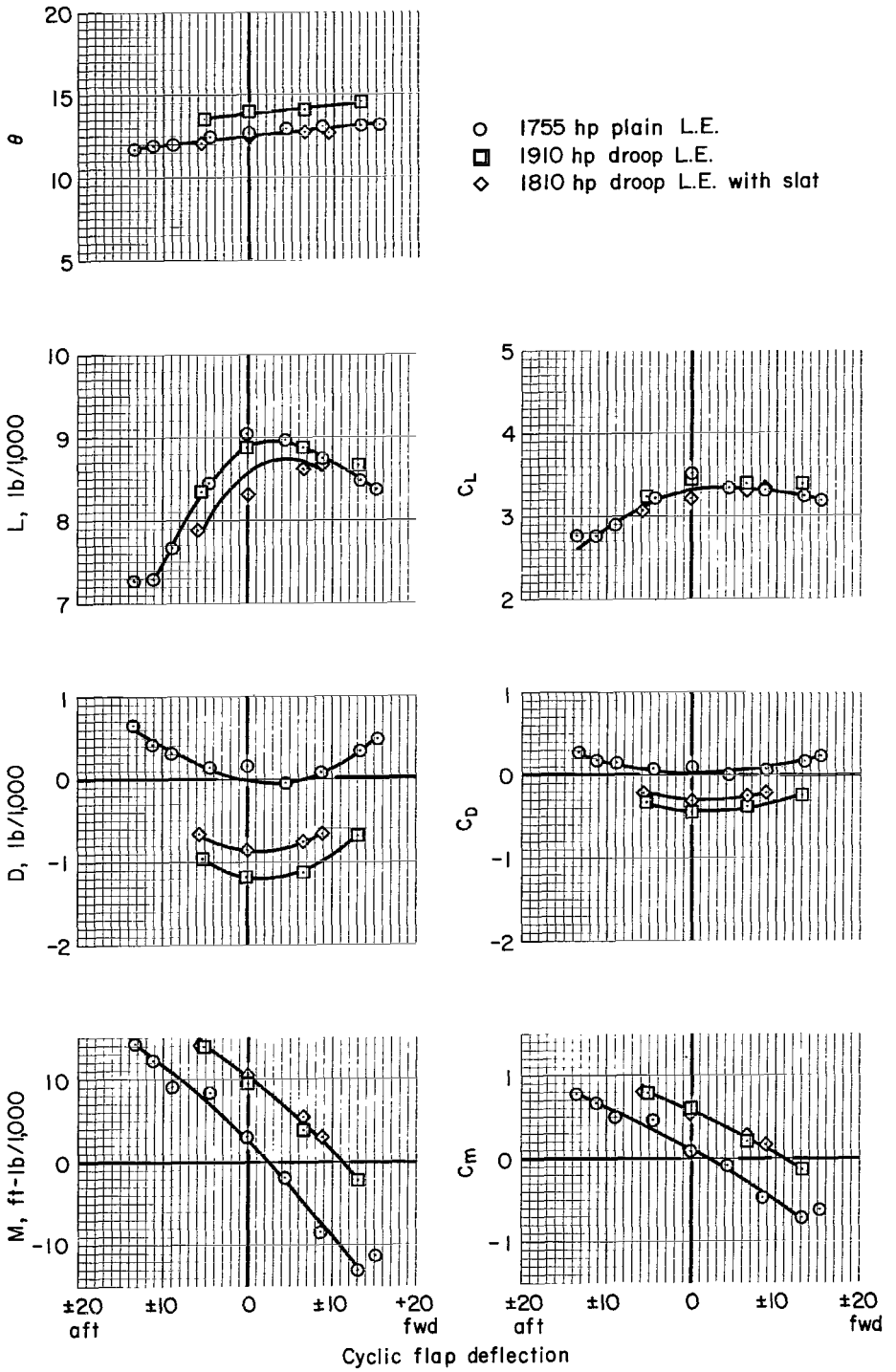

(a) Lift, drag, and pitching moment.

Figure 12.- Longitudinal rotor control effectiveness; $\tau = 20^{\circ}$, $\delta_e = 0$, $\delta_f = 40^{\circ}$, V = 59 knots.

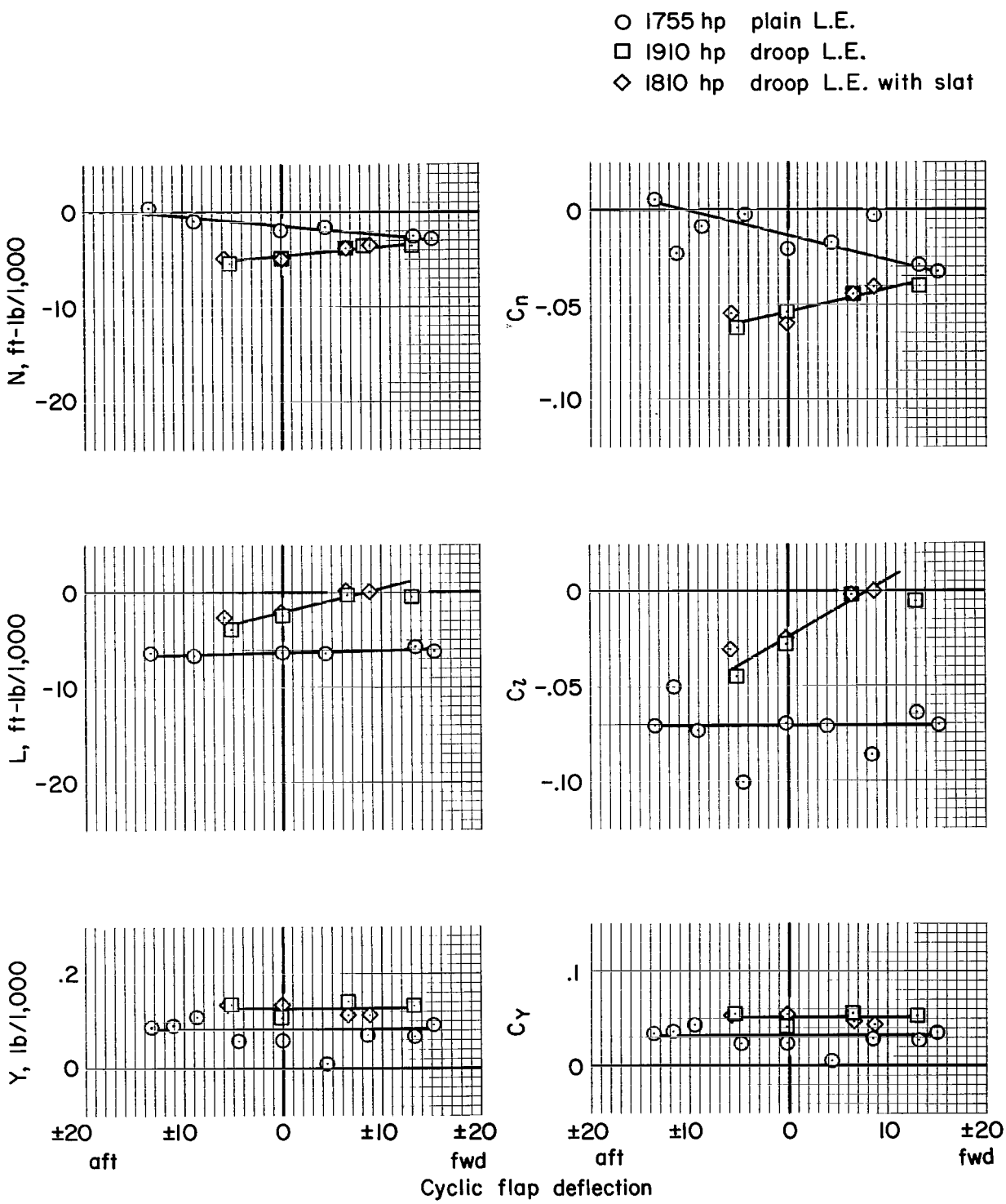

(b) Yaw, roll, and side force.

Figure 12.- Concluded.

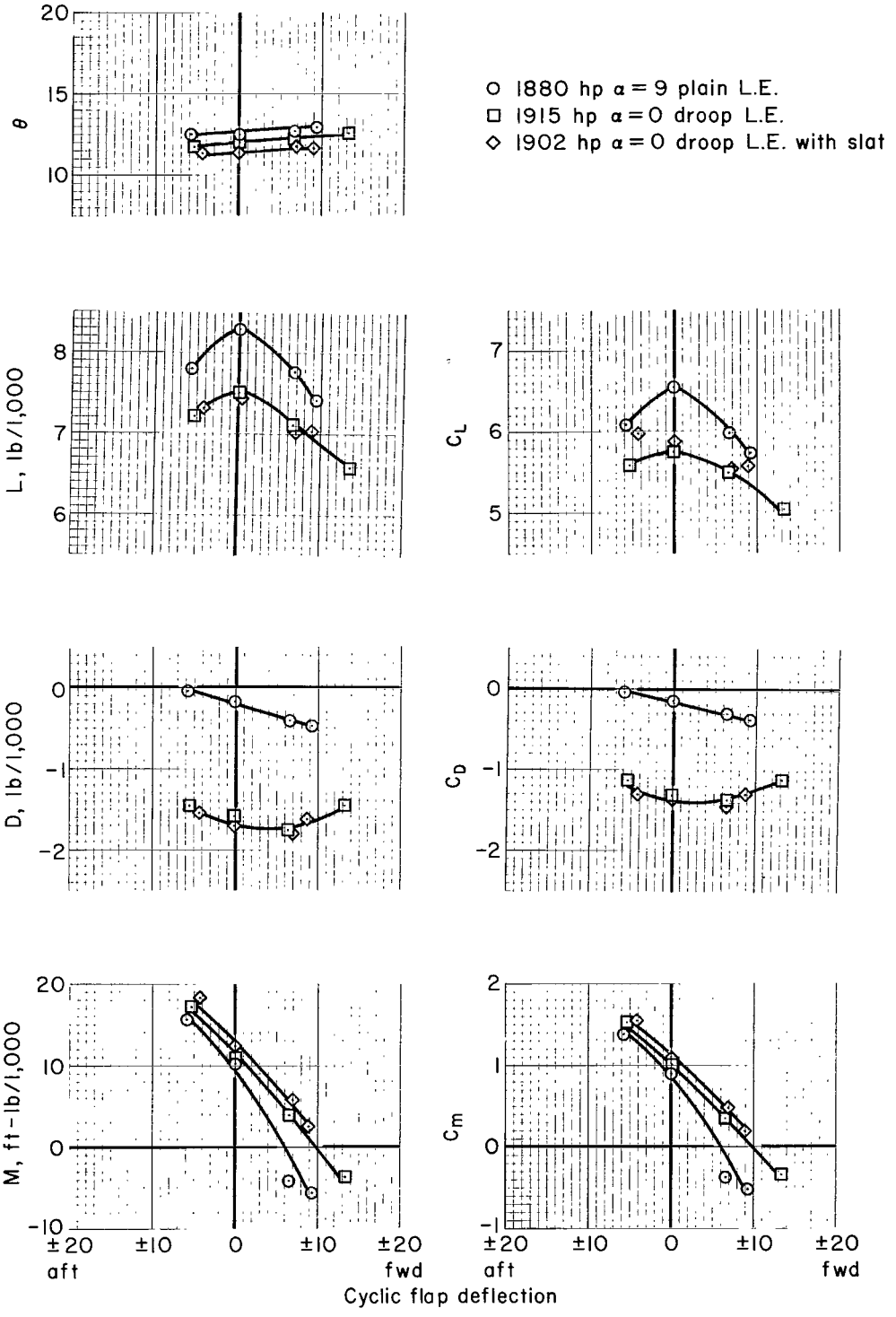

(a) Lift, drag, and pitching moment.

Figure 13.- Longitudinal rotor control effectiveness; $\tau = 30^{\circ}$, $\delta_e = 0$, $\delta_f = 40^{\circ}$, V = 39 knots.

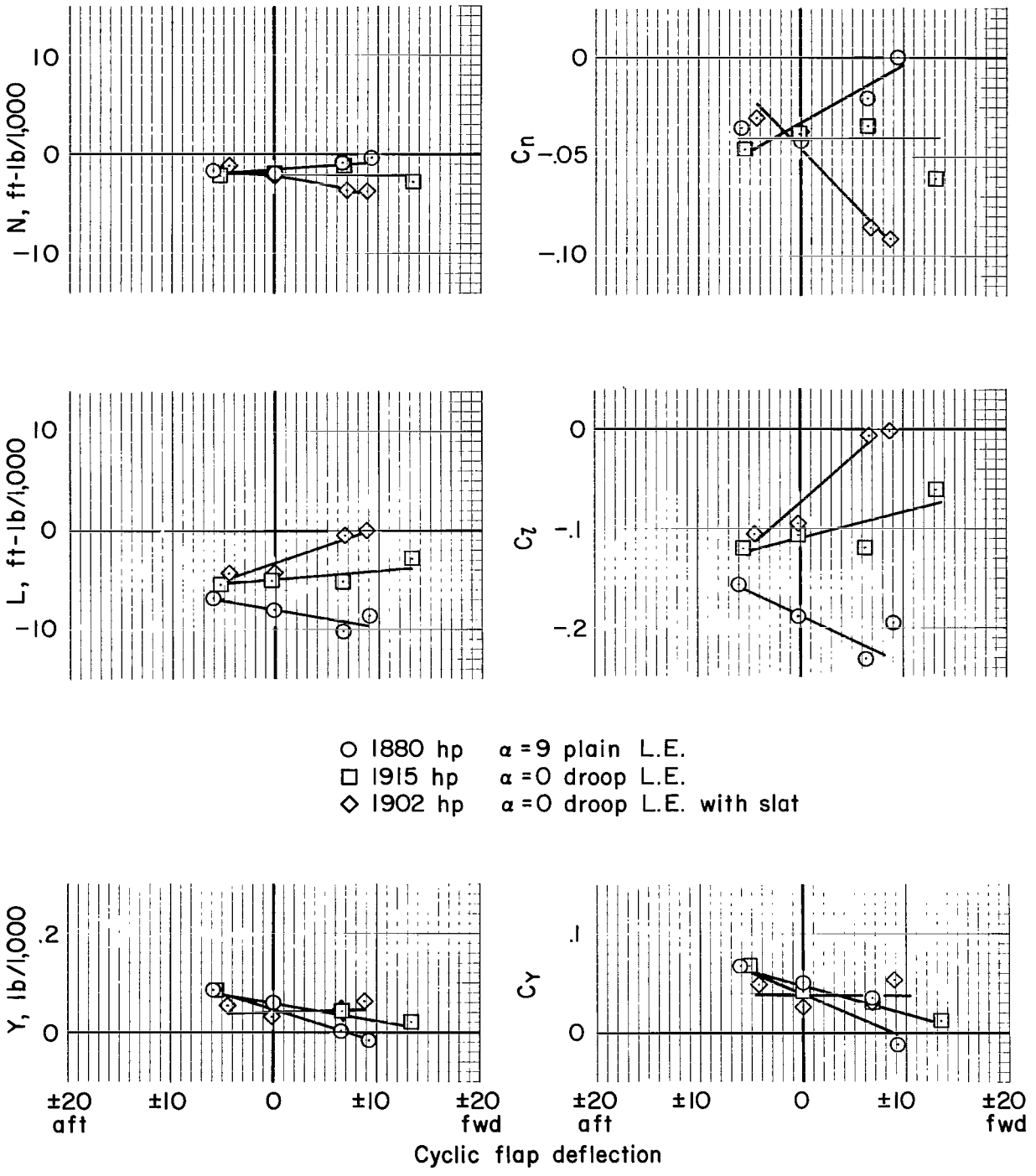

(b) Yaw, roll, and side force.

Figure 13.- Concluded.

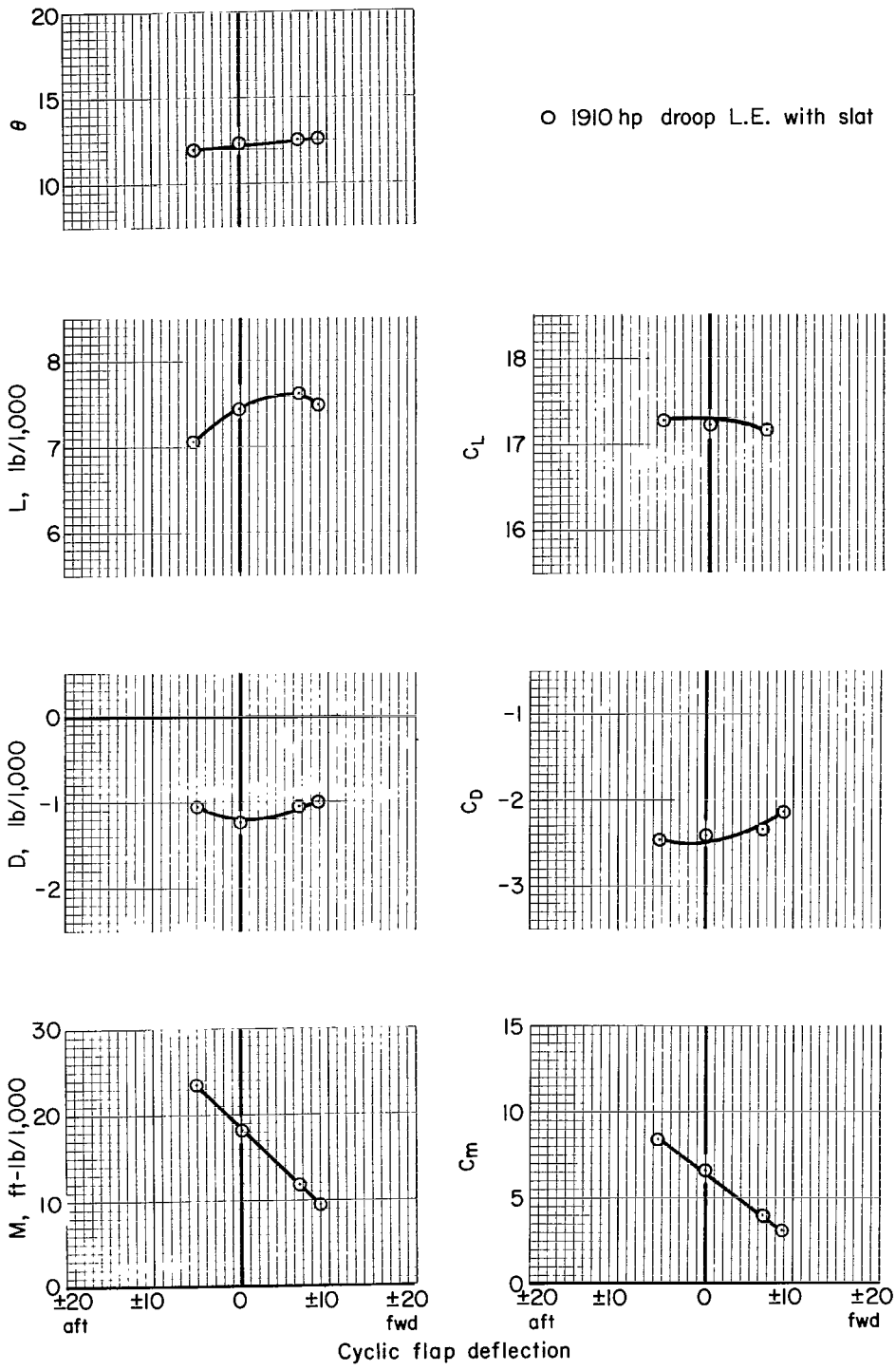

(a) Lift, drag, and pitching moment.

Figure 14.- Longitudinal rotor control effectiveness; $\tau = 50^{\circ}$, $\delta_e = 0$, $\delta_f = 40^{\circ}$, V = 22 knots.

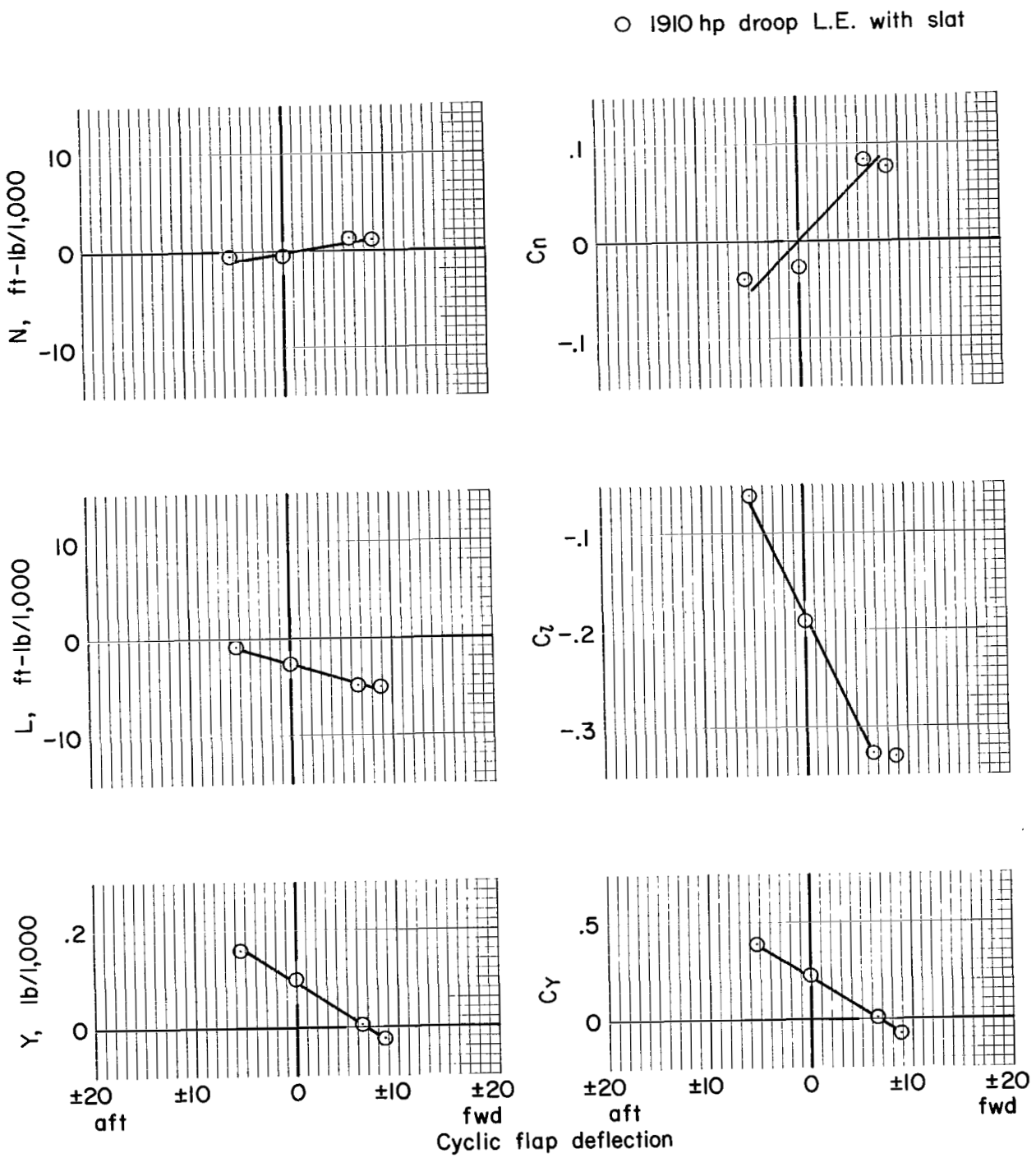

(b) Yaw, roll, and side force.

Figure 14 - Concluded.

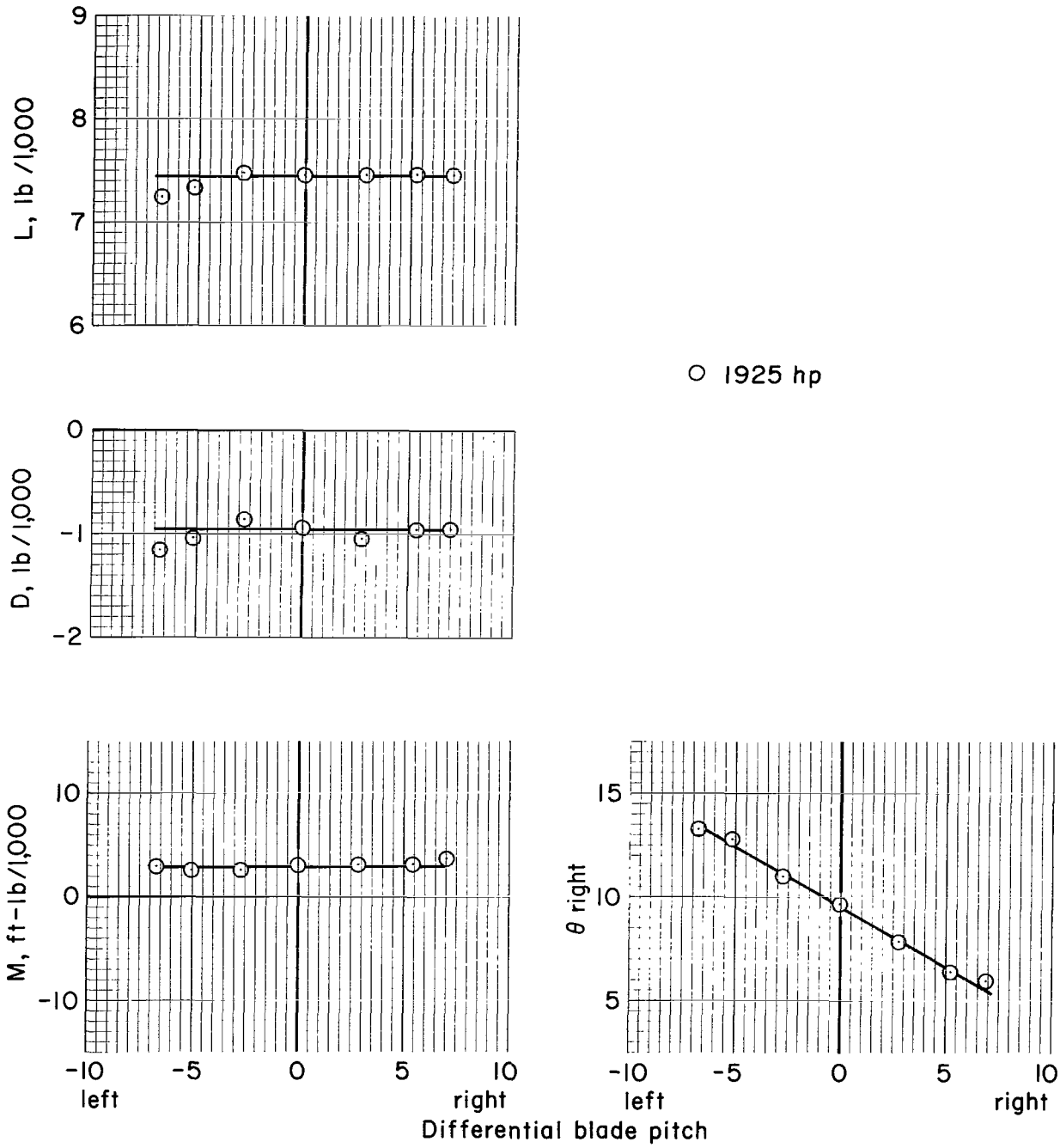

(a) Lift, drag, and pitching moment.

Figure 15.- Lateral rotor control effectiveness of the airplane on the static stand; plain L.E., $\tau = 62.2^{\circ}$, $\delta_f = 40^{\circ}$, $\alpha = 14.1^{\circ}$.

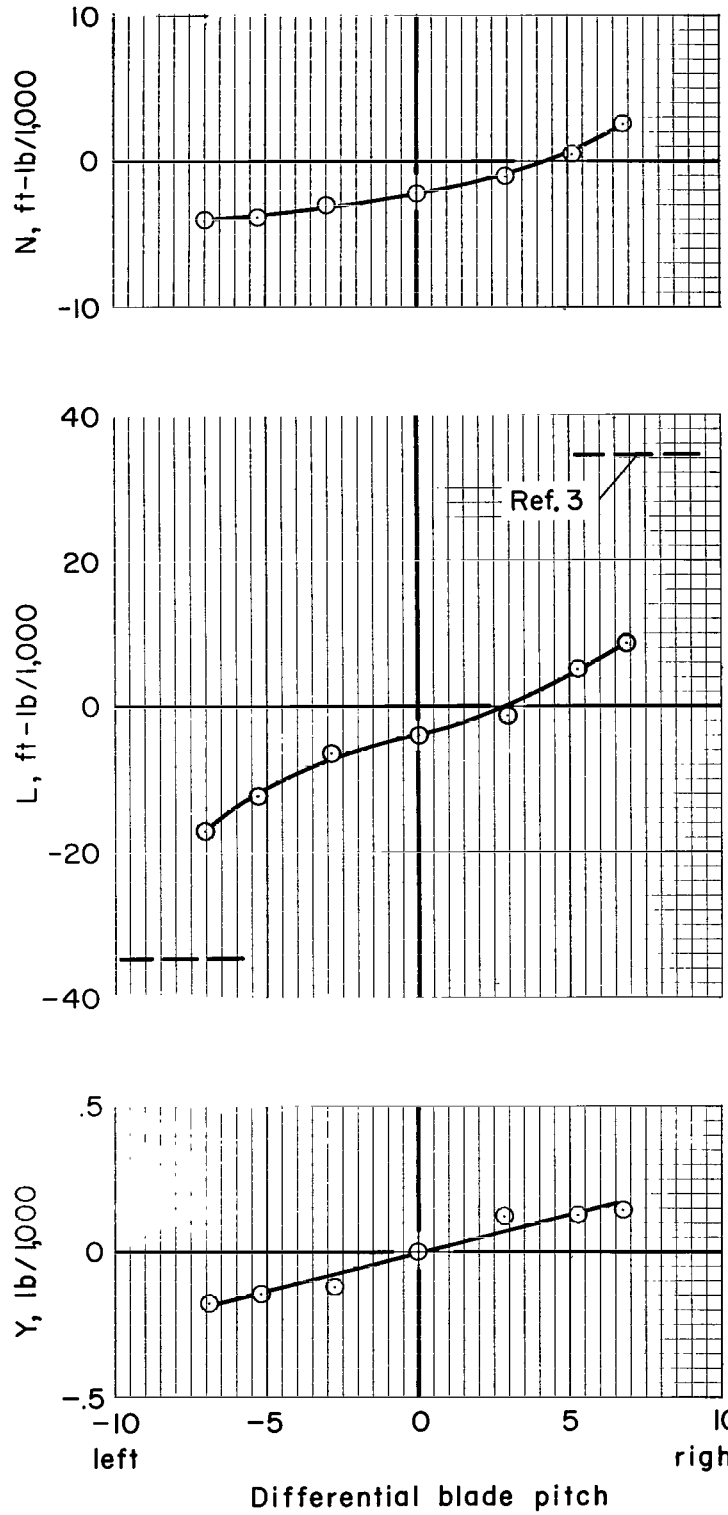

(b) Yaw, roll, and side force.

Figure 15.- Concluded.

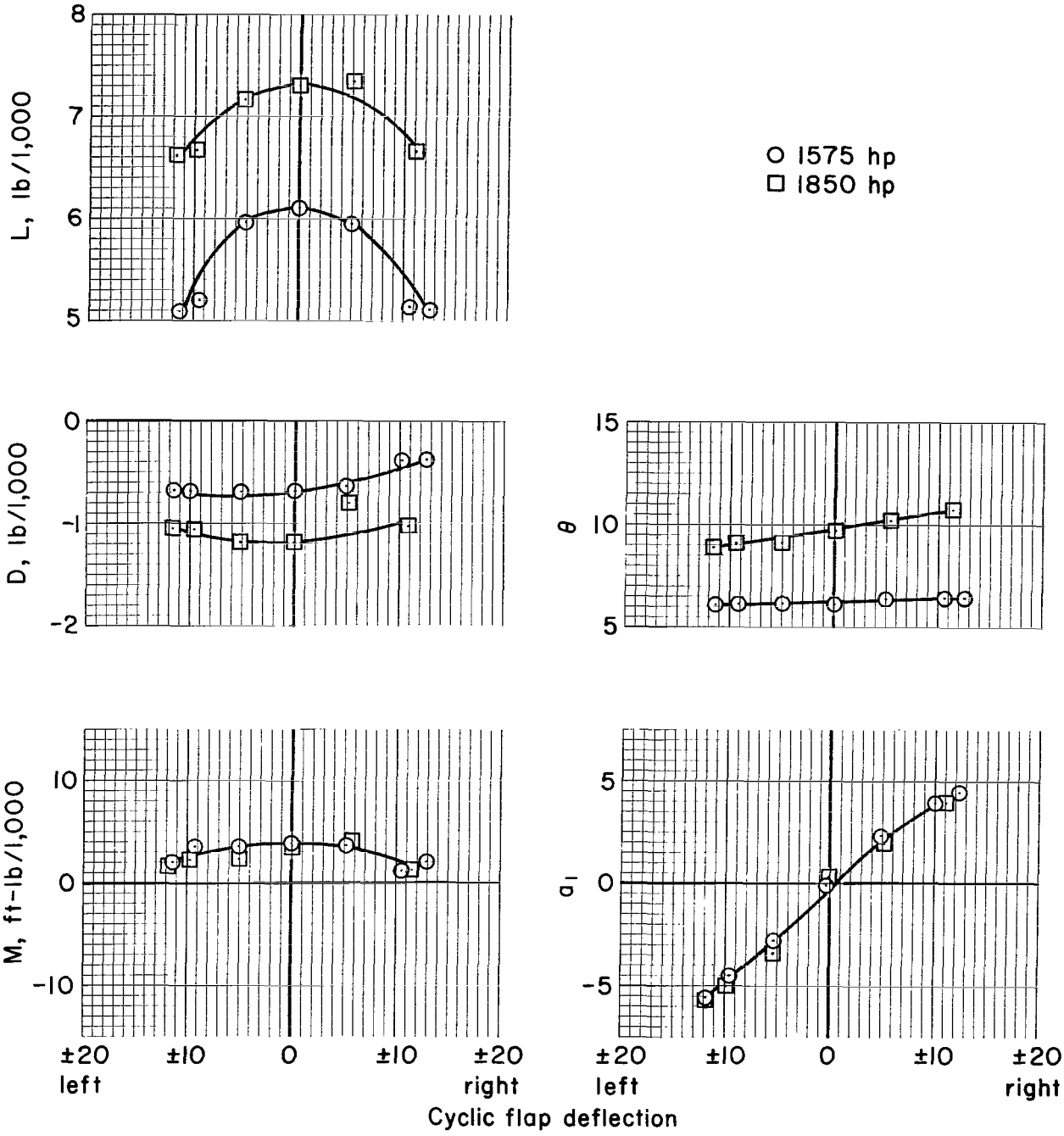

(a) Lift, drag, and pitching moment.

Figure 16.- Directional rotor control effectiveness of the airplane on the static stand; plain L.E., $\tau = 62.2^{\circ}$, $\delta_f = 40^{\circ}$, $\alpha = 14.1^{\circ}$.

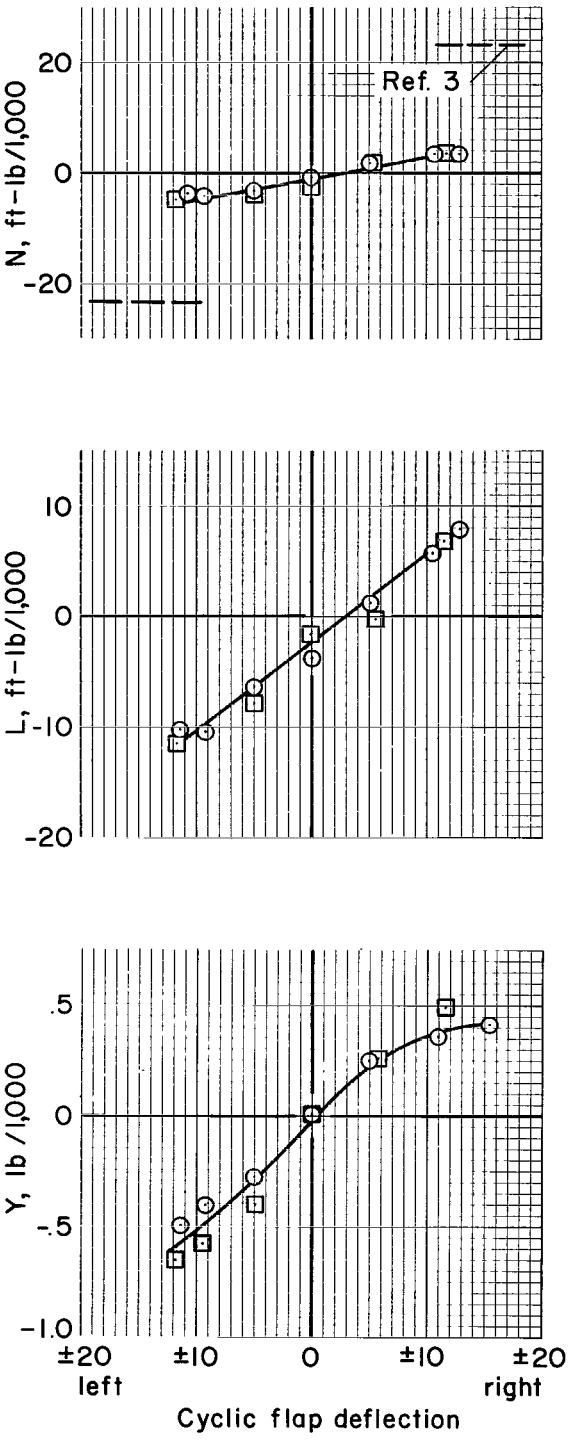

(b) Yaw, roll, and side force.

Figure 16.- Concluded.

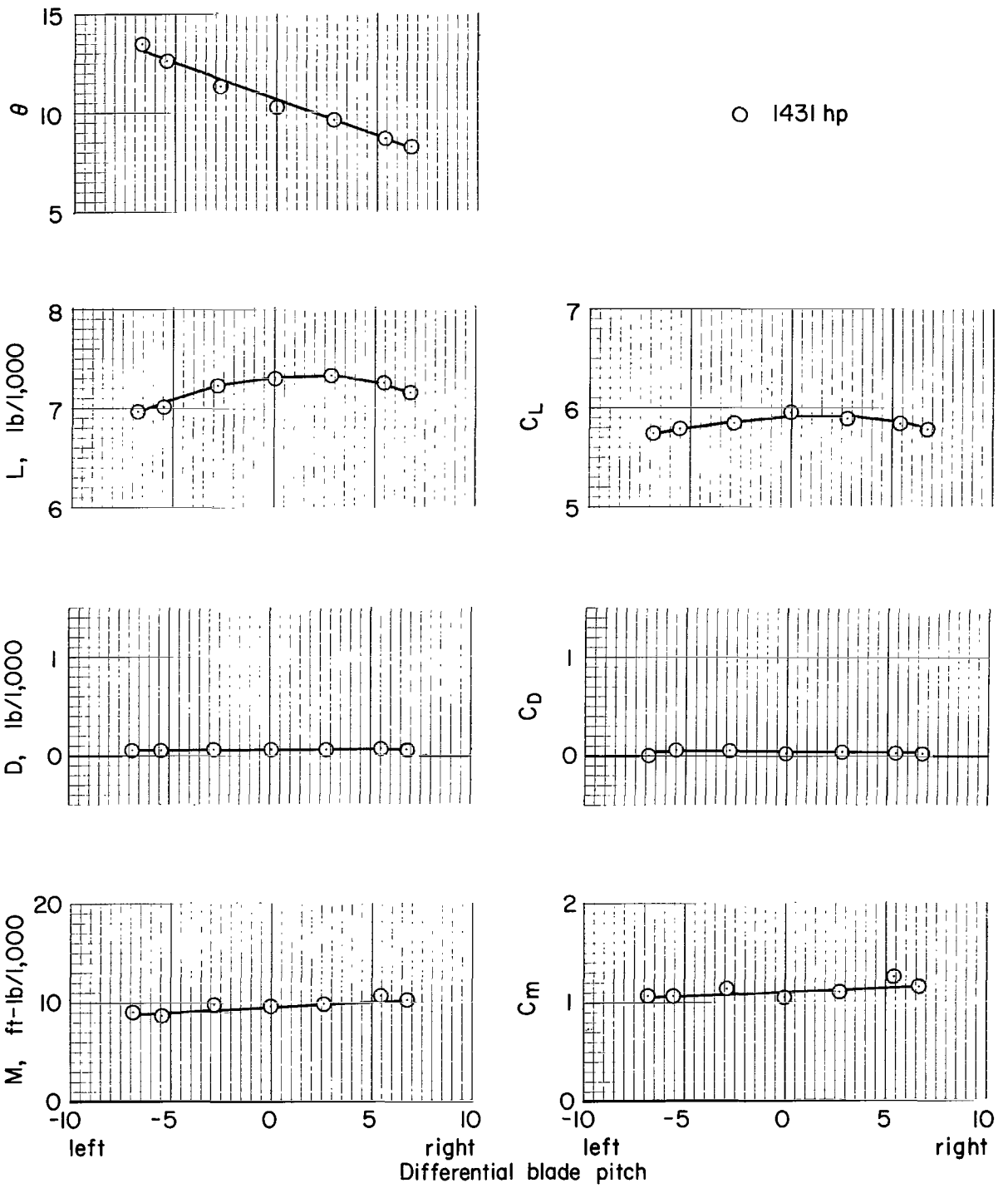

(a) Lift, drag, and pitching moment.

Figure 17.- Lateral rotor control effectiveness; plain L.E., $\tau = 40^{\circ}$, $\delta_r = 0$, $\delta_f = 40^{\circ}$, $\alpha = 0$, V = 39 knots.

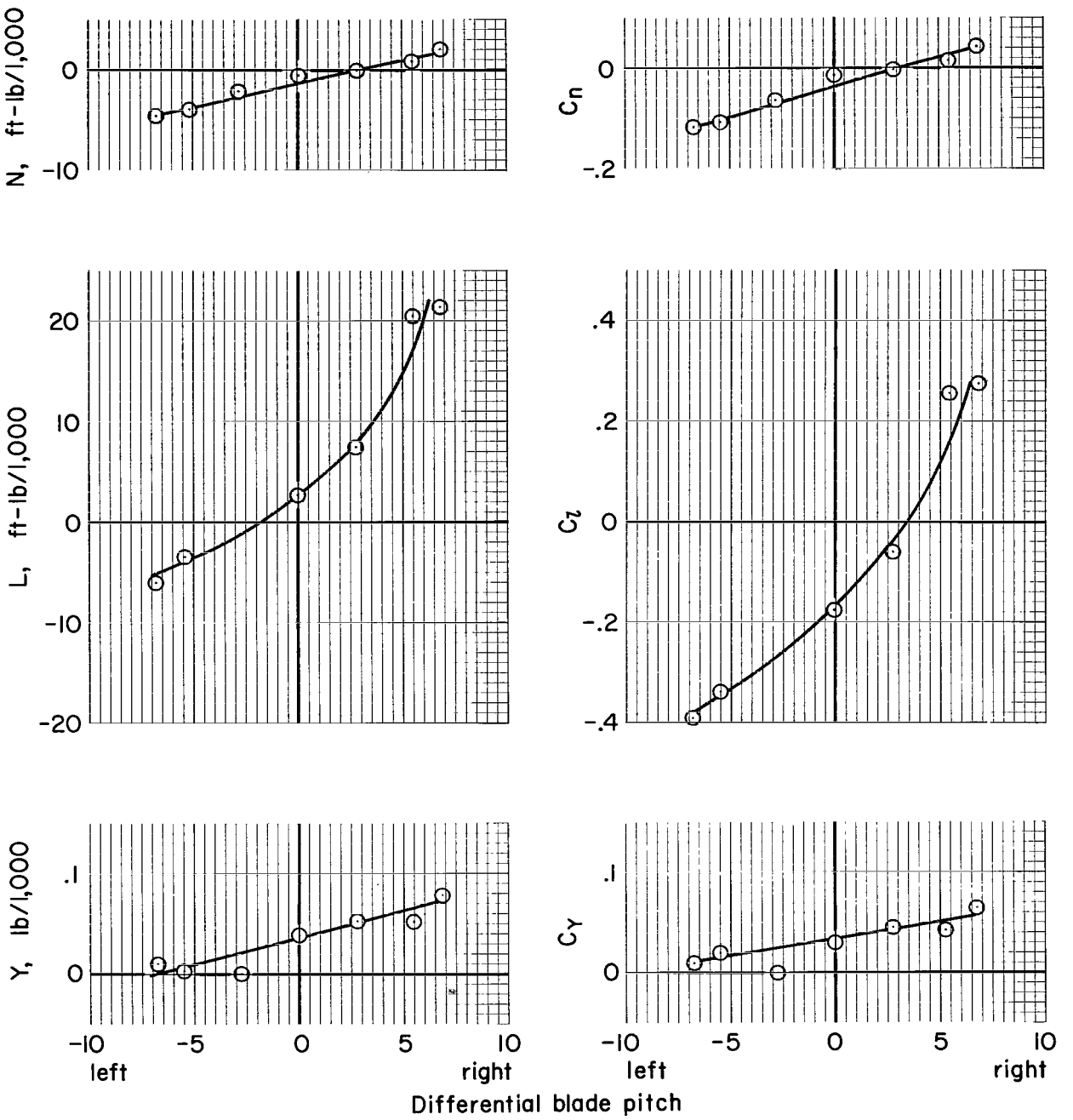

(b) Yaw, roll, and side force.

Figure 17.- Concluded.

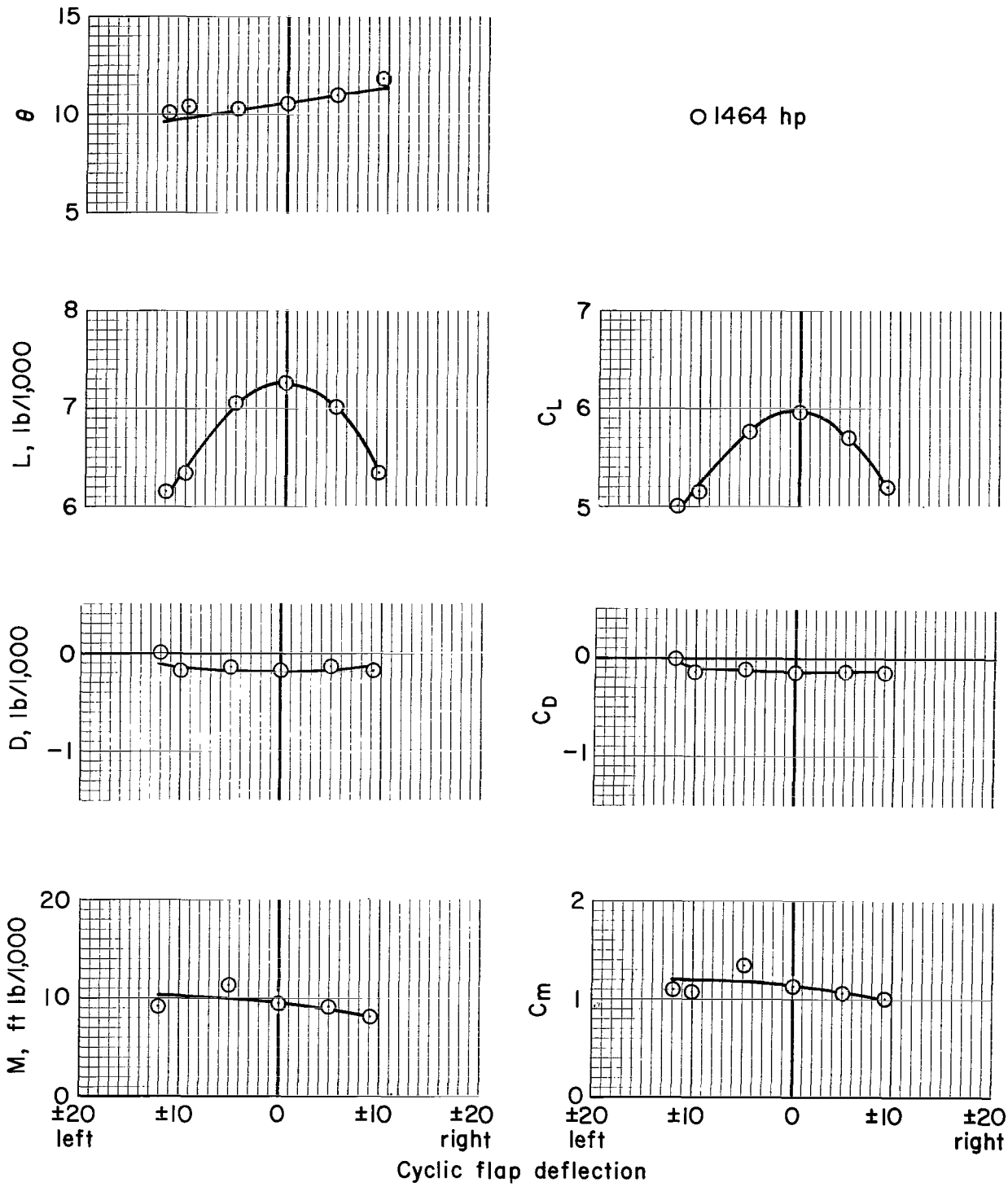

(a) Lift, drag, and pitching moment.

Figure 18.- Directional rotor control effectiveness; plain L.E., $\tau = 40^{\circ}$, $\delta_r = 40^{\circ}$, $\delta_f = 40^{\circ}$, $\alpha = 0$, V = 39 knots.

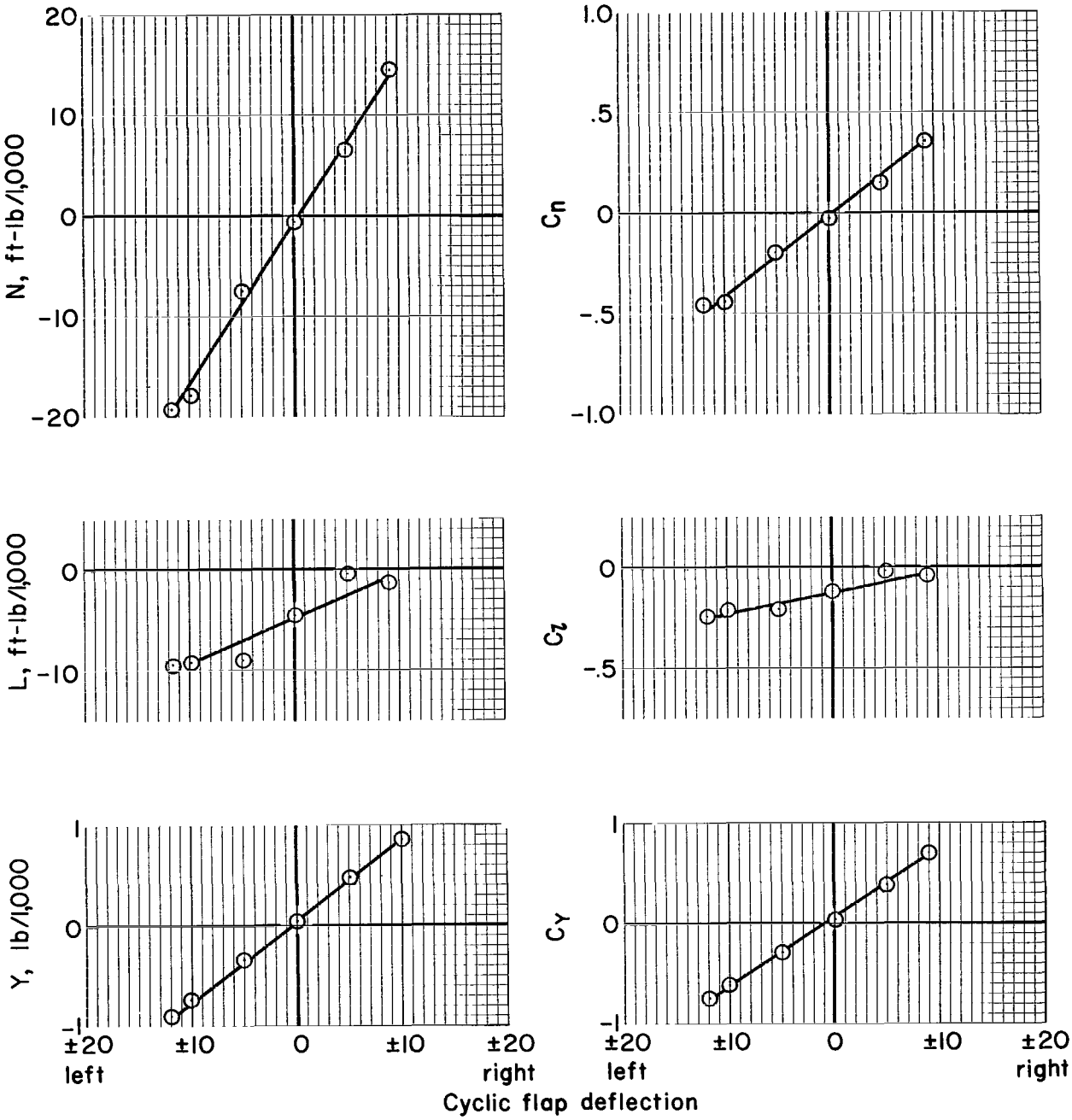

(b) Yaw, roll, and side force.

Figure 18.- Concluded.

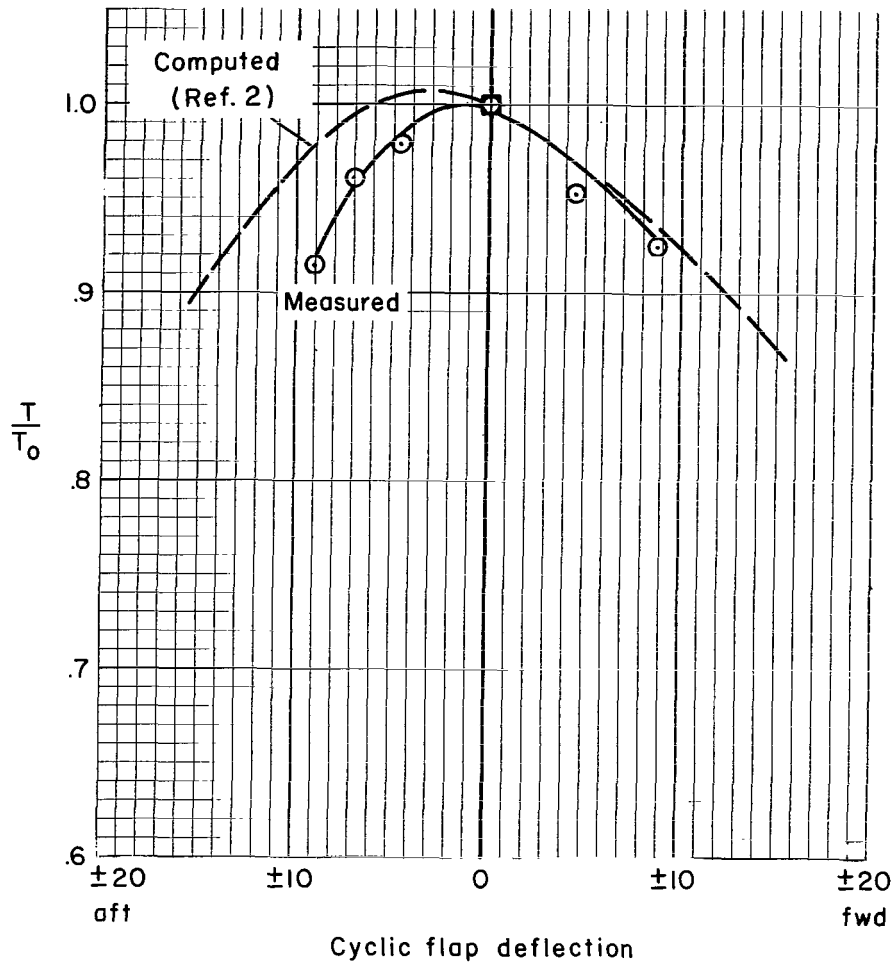

Figure 19.- Comparison between measured and computed thrust variation with control input; $\tau = 30^{\circ}$, $\delta_o = 11.7^{\circ}$, V = 40 knots.

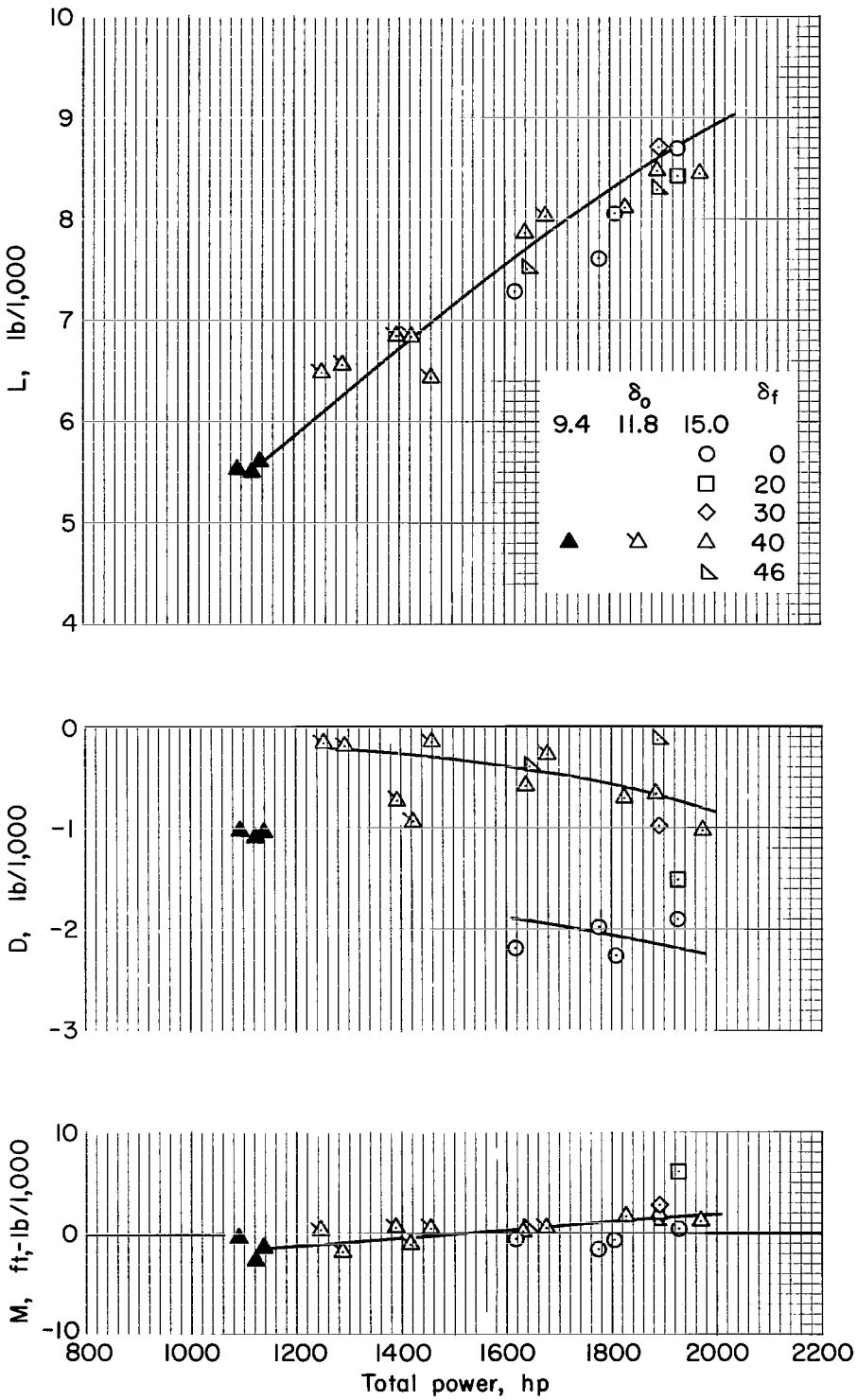

Figure 20.- Aerodynamic characteristics of the airplane on the static stand; plain L.E., $\tau = 62.2^{\circ}$, $\alpha = 14.1^{\circ}$.

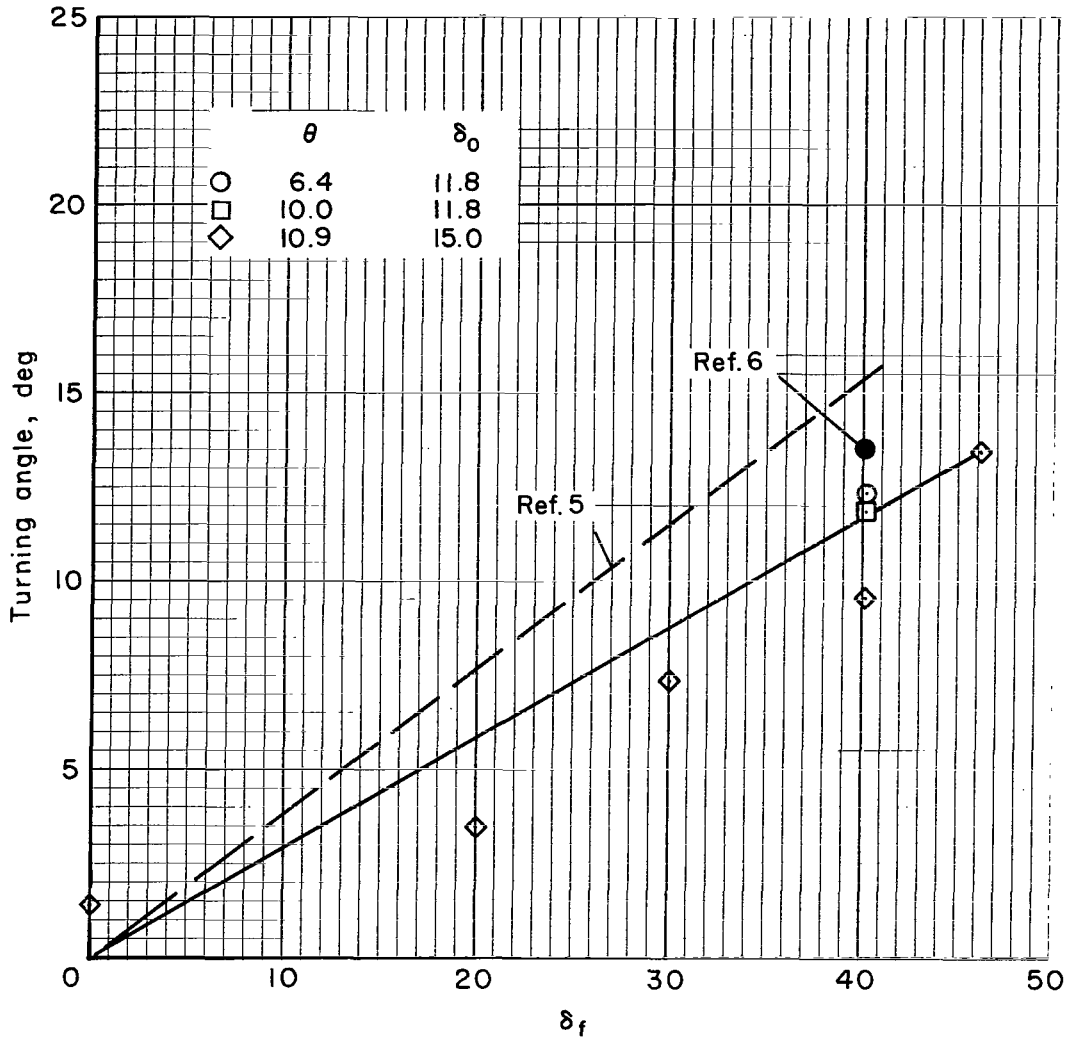

Figure 21.- Variation of turning angle with flap deflection; $\tau = 62.2^{\circ}$, $\alpha = 14.1^{\circ}$.

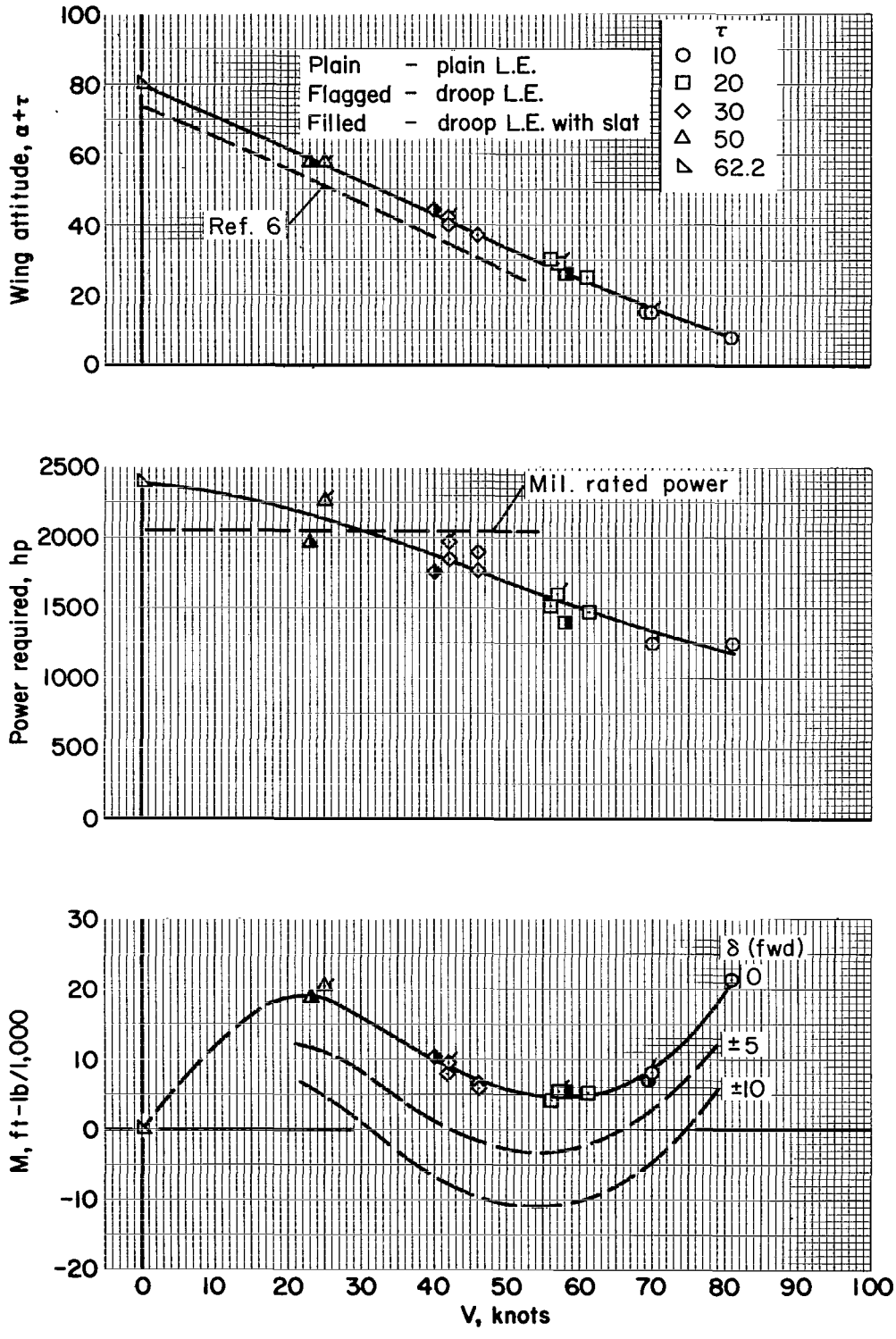

Figure 22.- Wing attitude, power, and control requirements in the transition; 9300 lb G.W., $\delta_f = 40^\circ$, $\delta_o = 11.7^\circ$, 700 rpm.

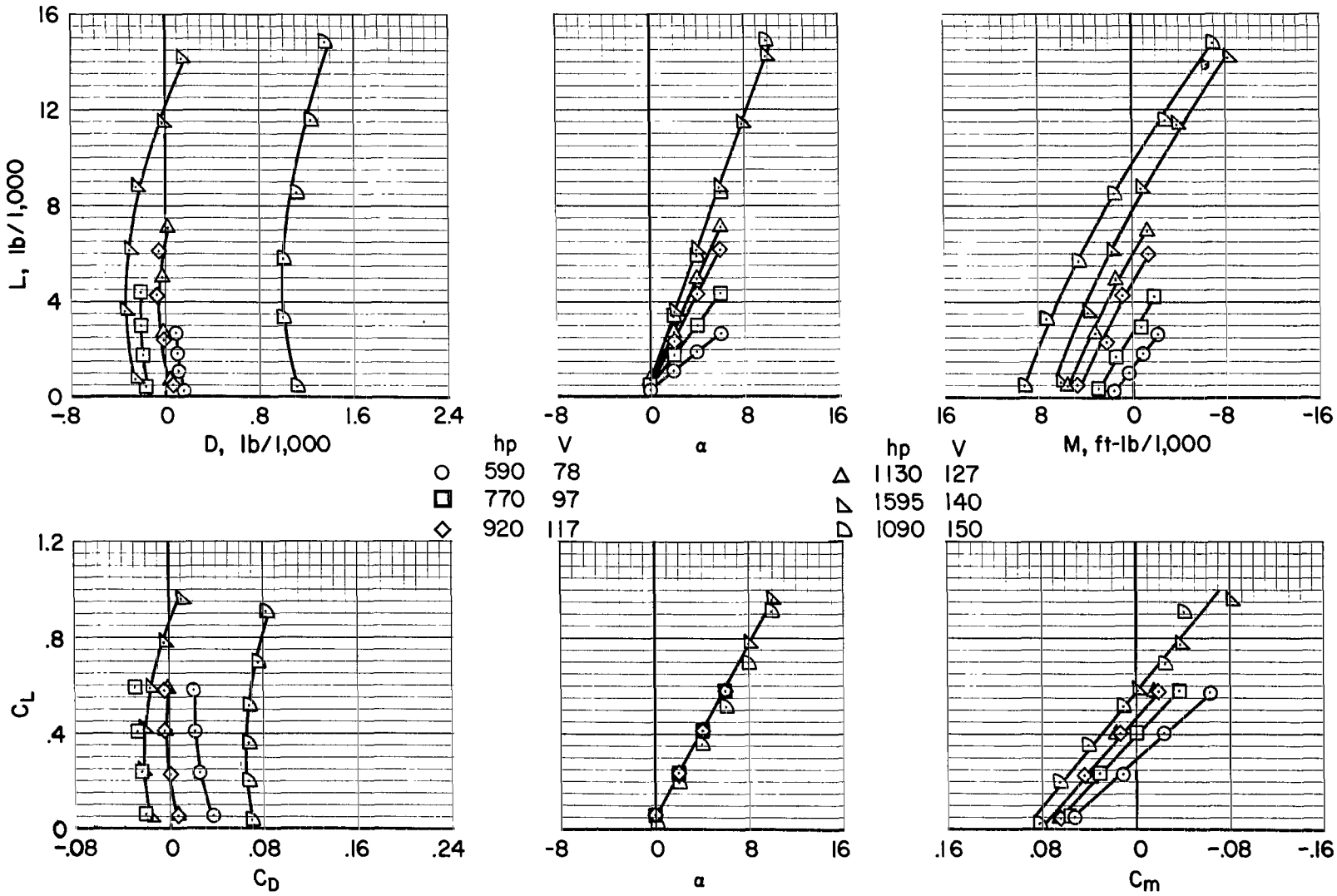

Figure 23.- Longitudinal characteristics of the airplane; plain L.E., $\tau = 0$, $\delta_f = 0$, $\delta_o = 2.3^o$, 700 rpm.